1. AGENCY USE ONLY (Leave blank)	2. REPORT DATE	3. REPORT TYPE AND DATES COVERED
	10 December, 1992	Final Report (15 July 89-14 Oct. 92)

4. TITLE AND SUBTITLE
Nondestructive Evaluation of Grain Size Distributions Using Multifractal Analysis of Backscattered Ultrasonic Signals

5. FUNDING NUMBERS
N00014-89-J-3106
uri5001---03

6. AUTHOR(S)
N. Bilgutay, B. Onaral and D. Nicoletti

7. PERFORMING ORGANIZATION NAME(S) AND ADDRESS(ES)
Electrical and Computer Engineering Dept.
Drexel University
32nd & Chestnut Streets
Philadelphia, PA 19104

8. PERFORMING ORGANIZATION REPORT NUMBER

9. SPONSORING/MONITORING AGENCY NAME(S) AND ADDRESS(ES)
Office of Naval Research
Physics Division - Code 1112
800 N. Quincy Street
Arlington, VA 22217-5000

10. SPONSORING/MONITORING AGENCY REPORT NUMBER

11. SUPPLEMENTARY NOTES
This report is a summary of D. Nicoletti's Ph.D. thesis and the joint publications of the authors in (6) related to sponsored research.

12a. DISTRIBUTION/AVAILABILITY STATEMENT
Approved for public release. Distribution unlimited.

12b. DISTRIBUTION CODE

13. ABSTRACT (Maximum 200 words)

Grain size is one of the factors which influence mechanical properties of metals like strength and fracture toughness. Ultrasonic waves propagating in polycrystalline materials are subject to attenuation dominated by grain boundary scattering. The importance of grain size estimation for industrial applications warrants the investigation of alternative methods of nondestructive grain size determination. Analysis of the power-law behavior of ultrasonic attenuation experimental data is used to link the wavelength dependence of the attenuation coefficient directly to the grain size distribution. The outcome is a simple relationship between the power-law which describes the grain size distribution and the power-law dependence of attenuation on wavelength. Justifications for the use of the power-law for the grain size distribution include scaling and self-similarity. Careful attention is given to the limitations in terms of a practical grain size distribution with finite limits. Two types of measurements are presented to verify the theoretical development: grain size distribution and ultrasonic attenuation. Nickel samples were prepared using three different annealing durations. The attenuation exponent is experimentally shown to be an appropriate nondestructive measurement of the grain size distribution exponent. Further scaling properties for different annealing durations are also explored. A nondestructive evaluation procedure is suggested for metal samples with identical grain size distribution exponents, where the shifts of the log-log representations of the attenuation curves can be used to characterize the different grain size distributions.

14. SUBJECT TERMS	15. NUMBER OF PAGES
grain size estimation, nondestructive characterization, ultrasonic attenuation, scaling, power-law relationship	44
	16. PRICE CODE

17. SECURITY CLASSIFICATION OF REPORT	18. SECURITY CLASSIFICATION OF THIS PAGE	19. SECURITY CLASSIFICATION OF ABSTRACT	20. LIMITATION OF ABSTRACT
unclassified	unclassified	unclassified	

FINAL TECHNICAL REPORT SUBMITTED TO THE OFFICE OF NAVAL RESEARCH PHYSICS DIVISION

Title: Non-Destructive Evaluation of Grain Size Distributions Using Multifractal Analysis of Backscattered Ultrasonic Signals

R&T #: uri 5001---03

Contract #: N00014-89-J-3106

Duration: July 15, 1989 - October 14, 1992
(Includes a 3 month No-Cost Extension)

Submitted: December 10, 1992

Scientific Officer: Dr. Logan E. Hargrove
Physics Division Code 1112

Investigators: Dr. Nihat M. Bilgutay (PI) and Dr. Banu Onaral
Electrical and Computer Engineering Department
Drexel University
Philadelphia, PA 19082
(215) 895-1269

Table of Contents

I. Introduction

Grain size is one of the factors influencing mechanical properties of metals like strength and fracture toughness, and has been widely used for monitoring product quality during manufacturing processes. Ultrasonic waves propagating in polycrystalline materials, such as metals, are subject to attenuation often dominated by grain boundary scattering. The strong correlation between ultrasonic attenuation and grain size has been well established and extensively utilized in recent years for grain size estimation because it is practical, relatively inexpensive, and most significantly nondestructive. However, the fundamental mechanisms underlying the empirical correlation between ultrasonic scattering measurements and microstructure are highly complex and lack a satisfactory theoretical model. Current practical techniques for material characterization and grain size estimation are generally based on simplified scattering models and often can serve only limited purposes.

The importance of grain size estimation for industrial applications warrants the investigation of alternative methods of relating ultrasonic attenuation to grain size. The property known as scaling, which can be broadly defined as adjustments according to a proportion, will be defined both mathematically and through examples. The application of scaling behavior for the interpretation of ultrasonic attenuation experimental data will be investigated and related to the microstructural properties of the material samples. Although the average grain size contains valuable information related to the mechanical properties of the material, the distribution of grain size can significantly affect the interpretation of experimental results [Smith et. al. 1981]. It follows that the knowledge of the grain-size distribution can be valuable information for microstructure characterization. Relevant scaling concepts will be reviewed and then used to link the wavelength dependence of the attenuation coefficient extracted from experimental data directly to the grain-size distribution.

The contributions of this work begin with the hypothesis of a new scaling relationship between the grain-size distribution and attenuation. The outcome of the theoretical development is a straightforward relationship between an exponent to describe the grain-size distribution and the power-law dependence of attenuation on wavelength. This establishes the first straightforward relationship between the grain-size distribution function and the exponent that characterizes the dependence of attenuation on wavelength, linking the microstructural properties to the dynamical response.

An experiment to verify this relationship for nickel samples is outlined in section V, and the results are presented in section VI. A second scaling relationship is examined for the annealing durations in section VI.D. The conclusions are discussed along with suggestions for future directions in section VII.

The work reported here is a result of interdisciplinary cooperation of laboratories from Drexel University: the Signal Processing Laboratory, supervised by Drs. Nihat Bilgutay and Banu Onaral, and the Metallographic Laboratory, supervised by Dr. Samuel Nash, as well as laboratories supervised by Dr. E. R. Generazio from the NASA Lewis Research Center.

II. Review of Grain Size Considerations

A. Measurement of Average Grain Size and Grain Size Distributions

The accurate measurement of grain size is a continuing topic of research, even when it is accomplished destructively using polishing, etching and photomicrographs of the grain boundary structure. The most commonly used techniques for average grain size measurement are the line intercept method and the American Society for Testing Materials (ASTM) comparison method [DeHoff 1968 p. 233]. The line intercept approach uses a grid placed over the photomicrograph and determines the average number of times test lines intersect the boundaries. The alternative

method compares the photomicrograph to ASTM grain size charts. Both of these techniques are highly subjective measurements; line intercept results have been shown to vary as much as 50 per cent [DeHoff 1968 p. 250].

This work requires the measurement of the grain-size distribution, not just the average grain size. The distinction between average grain size and grain-size distribution measurement broaches an important criticism of past work. Ultrasonic attenuation is proportional to the volume of the scatterer for one scattering region, the Rayleigh region. In cases where there is a distribution of grain sizes, the third statistical moment of the grain-size distribution should be used in the analysis of this type of scattering. Researchers have used the third power of the average for the third moment [Klinman & Stephenson 1981], an equality that may not be valid when a grain-size distribution exists. In some cases, this use of the average may be due to the investigators using the intercept method for grain size determination, which provides only the average size [Mercier 1975, Klinman & Stephenson 1981, Saniie & Bilgutay 1986].

The effect of the distribution of grain sizes on mechanical properties of the metal has been suggested, specifically that conventional experimental interpretation may not be correctly considering the "uncontrolled and unrecognized variations in the grain-size distributions." [Rhines & Patterson 1982] The authors also state that "The near absence of recognition of these features and of their effects on properties is understandable in view of the great amount of labor required in the experimental measurement of grain volume distribution, together with the fact that the distributions are not particularly noticeable in microstructures seen two-dimensionally." [Rhines & Patterson 1982]

One recent innovation in the determination of the grain-size distribution is the use of two-dimensional Fourier transforms of an image of the grain boundaries [Generazio 1988b]. This method is briefly reviewed below since it is used for the experimental work reported here.

A photomicrograph of the grain boundaries is first digitized using a 512 by 512 pixel array, circularly masked, and then the grain boundaries are enhanced digitally. The grains are tone-pulse-encoded for Fourier domain measurement of the grain sizes as follows: beginning at the center of the image and proceeding outwards along a radial line, 3 periods of a sine wave are fitted into the width of each grain crossed by the radial line. This creates a tone-pulse-encoded set, whose Fourier transform reveals the density function for the widths (or size) of the grains. A one-dimensional example of tone-pulse encoding is shown below in Figure 1. This process is carried out for a fixed number of radial lines circling the micrograph. A two-dimensional density function dependent on size and angle is created. If the grain-size distribution is isotropic, then the histogram will be independent of angle.

A test case for this method [Generazio 1988b] utilized an image with a known distribution of circles. The algorithm correctly measured the size distribution for the larger grains, but it deviated for the smaller grains. This is easily understood by analyzing how the circles are tone-pulse encoded. Figure 1 is clearly an ideal case: the circles are encoded along their diameter, the longest chord of the circle. However, as the size distribution measurement is taken along another radial line, the chord will not be the diameter, and the measurement will give additional, misleading weighting to smaller sized grains. Consequently, the size measurement for the smaller grains is expected to have a higher degree of uncertainty than the measurement for the larger grains.

The percent uncertainty in the grain size measurement [Generazio 1988b] can be calculated as follows:

$$\text{percent uncertainty} = \left| \frac{3 \text{ pixels}}{\partial} \right| * 100 \text{ per cent} \qquad (1)$$

where ∂ is the grain size and 3 pixels is the experimental uncertainty based on the size of the grain boundary on the micrograph. This expression provides another reason why the measurement is more accurate for larger grain sizes; the smaller the grain, the larger the percent uncertainty.

Additionally, since the Nyquist rate [Oppenheim & Willsky 1983, p. 519] must be satisfied, the smallest number of pixels that can be used to encode a three-cycle sine wave is ten. This observation sets the lower limit for the grain size that can be resolved using this technique.

II.B. Distribution Functions Used For Grain Size

It will be shown that the attenuation coefficient can be related to the grain-size distribution function, N(D) defined as

$$N(D)\,dD = \text{the number of grains of size between D and D + dD}$$

It is often difficult to assign a mathematical formula for the distribution function, especially when only a few data points are known, as is the case for many grain size measurements.

The log-normal distribution has been used for grain size in metals, based on measurements with twelve values [Feltham 1957], and [Seemann & Bentz 1954] (German text) as reported in [Papadakis 1961]. It is interesting to note that one author [DeHoff 1965] indicates that based on experimental results the distribution must be skewed and that the log-normal is not the only possible distribution function; it simply "provides a versatile functional form . . . . In the absence of additional information, it is recommended that this form be used . . . ." [DeHoff 1965].

The log-normal distribution has been used for many other applications, including body weights, rainfall, and electrical resistance in materials with random scatterers [West & Shlesinger 1989]. It is one of a class of distributions used for systems comprised of many components. It has been shown that there is a connection between the log-normal and another distribution applicable to many-component systems, the power-law distribution. The upper tail end of a log-normal distribution (the last two to three percentile region) can be approximated by an inverse power-law [West & Shlesinger 1989], as can a distribution with a large variance [Montroll and Shlesinger 1983]. While an inverse power-law expression was used for the grain-size distribution function in this work, it is interesting to keep in mind these relationships between the log-normal and power-law functions.

There is yet another connection between the log-normal and power-law distributions. The cumulative frequency of the grain weight, i.e., the percentage of grains which are less than or equal to a given weight, is often represented on the log-log scale [Rhines & Patterson 1982, Doherty 1984]. The linearity of this figure is designed to show that the volume distribution is log-normal; perhaps a simpler way of interpretation is to represent the volume distribution with a power law.

III. Ultrasonic Attenuation

A. Introduction

The ultrasonic wave traveling through a solid is subject to scattering and absorption which results in energy losses. As the ultrasonic burst advances through homogeneous material, its amplitude is attenuated as

$$p = p_0 e^{-\alpha d} \tag{2}$$

where p_0 is the initial pressure, p is the pressure at d, the distance traveled, and α is the pressure attenuation coefficient in Nepers per centimeter (Np/cm) [Krautkramer & Krautkramer 1983 p. 108]. In general, the attenuation coefficient can be a function of wavelength (λ) and size of the scatterer (D) and can be expressed as

$$\alpha = \alpha_a + \alpha_{sc} \tag{3}$$

where α_a is the absorption term and α_{sc} is the scattering loss associated with grain boundaries. Since wavelength and frequency (f) are related through the velocity of propagation c (cm/sec):

$$c = f\lambda \tag{4}$$

the attenuation can also be expressed in terms of its frequency dependence.

Absorption in metals is caused primarily by the inelastic behavior of the materials, dislocation damping, and magnetic domain damping [Papadakis & Reed 1961, Smith 1987]. The dependence of the absorption loss on frequency is usually presumed to be linear [Roth 1948]. Many researchers have assumed that the grain scattering loss at ultrasonic frequencies is so large relative to the absorption loss that the latter is negligible [Papadakis 1970, Serabian & Williams 1978, Bozorg-Grayeli 1981 p. 16, Smith et. al. 1981]. One attempt to justify this assumption experimentally [Wegel & Walther 1935] used different materials, most notably copper. Ultrasonic attenuation measurements were made before and after annealing. Since the copper before annealing has little or no grain boundaries, the dissipation of energy was due to absorption. After annealing, the dissipation immediately increases dramatically (by a factor of more than 16) due to recrystallization and the formation of grain boundaries. Unfortunately, there is a drawback to the use of this experiment as a means of justifying the assumption that grain boundary scattering dominates ultrasonic attenuation. The dislocations in the crystalline structure also change during annealing, and they contribute to the absorption term of the attenuation. Thus, it is impossible to separate the increase of the attenuation after annealing due to either formation of grain boundaries or change of the dislocations. This work is therefore left with the assumption that the attenuation in the metal samples is due to grain boundary scattering alone; thus the notation for the attenuation will be $\alpha(\lambda,D)$ [i.e., $\alpha(\lambda,D) \approx \alpha_{sc}(\lambda,D)$].

A term linearly dependent on frequency has been previously added to the attenuation expression for some applications [Mason & McSkimin 1948]. This term assumably accounts for the power dependence deviating from four, as expected for Rayleigh scattering. In other developments, an f^2 term was used, again based on the frequency dependence differing from f^4 [Kumar & Govil 1980].

III.B. Attenuation Theory

1. Single Grain Size

Ultrasonic scattering formulas have been studied and classified into distinct scattering regions according to the ratio of the sound wavelength to the size of the grains. This section reviews some important results in detail for material with a single grain size or an average grain size. The review of the extension of the theory to a grain-size distribution [Smith 1982] follows in Section III.B.2. The assumptions used in the derivations can include:

- grains are weakly anisotropic (dependence on direction)
- there is no preferred orientation for grains
- grains are equiaxed or spherical
- material contains single-crystal grains of a single phase with no voids or inclusions

The theoretical development based on these assumptions relates the attenuation due to grain boundary scattering to wavelength, and in many cases to the dependence on elastic constants and

sound velocities of the material. It is reviewed in the section below that the attenuation is expected to vary as a function of wavelength (λ) and scatterer size (D) as follows:

$$\begin{aligned} &\text{Rayleigh Region:} && \alpha(\lambda,D) = C_r D^3 \lambda^{-4}, && \lambda \gg D \\ &\text{Stochastic Region:} && \alpha(\lambda,D) = C_s D\lambda^{-2}, && \lambda \approx D \\ &\text{Diffusive Region:} && \alpha(\lambda,D) = C_d/D, && \lambda \ll D \end{aligned} \quad (5)$$

where C_r, C_s, and C_d are constants of the material. For spherical grains, D is the diameter; in the case of nonspherically shaped grains, D is interpreted to be the largest measurement of the grain.

There have been numerous studies of the theoretical developments resulting in the expressions for the attenuation in Equation 5. Selected references are cited below, providing examples of approaches and assumptions used to derive the attenuation for the different scattering regions:

Table 1: References for Theoretical Approaches to Attenuation

a) $\lambda \gg D$, single scatterer, neglecting mode conversion	Rayleigh 1894
b) $\lambda \gg \overline{D}$, multiple scatterers, neglecting mode conversion	Mason & McSkimin 1947
c) $\lambda \gg \overline{D}$, multiple scatterers, using mode conversion	Lifshitz & Parkhomovskii 1950, Merkulov 1956, Bhatia 1959a, 1967, Bhatia & Moore 1959b
d) $\lambda \ll \overline{D}$, multiple scatterers	Mason & McSkimin 1948
e) all relative values of λ and D	Roney 1950
f) statistical signal processing	Saniie & Bilgutay 1986, Saniie et. al., 1988

III.B.2. Grain-Size Distributions

The effect of neglecting the grain-size distribution can be seen in the interpretation of experimental results. Some investigators have postulated that the ultrasonic attenuation is dominated by Rayleigh scattering and have used a fourth power dependence of attenuation on frequency in order to find the average grain size [Kumar & Govil 1980, Mercier 1975, Papadakis 1964, 1965a, 1965b, Roderick & Truell 1952, Smith et. al. 1981], despite measurements demonstrating that the power dependence has a noninteger exponent between 2 and 4 [Mason & McSkimin 1947, Papadakis 1970]. In other words, researchers have used the following relationship for the average grain size $(\overline{D})$ and frequency (f)

$$\alpha(f) \sim (\overline{D})^3 f^4 \quad (6)$$

with a certain degree of success, but this approach has proved unsatisfactory for some samples for two possible reasons. First, using the third power of the average grain size may not be valid when there is a distribution expression for the grain sizes. When a grain-size distribution exists, the attenuation is a function of the third statistical moment. Second, Rayleigh scattering requires that the wavelength is much greater than the size of the scatterers. Although the wavelengths chosen may be greater than the average grain size, they may in fact be comparable in size to the largest grain size, causing other scattering processes to occur. Thus one or both of the two terms of Equation 5 can be inappropriate for the dependence of attenuation on grain size and frequency.

The most developed application of grain-size distributions to attenuation was given in [Smith 1982], for which both Rayleigh and stochastic scattering was assumed to occur. The author began with Roney's expression for scattering for all wavelengths [Roney 1950 p. 14]

$$\alpha = \frac{2}{D\mu^2}\overline{\left(\frac{\Delta K}{K}\right)^2}\sum_{m=0}^{\infty}(2m+1)\sin^2\delta_m \qquad (7)$$

and used a probability density function for the grain diameters. The total attenuation per unit length due to all scatterers was found neglecting multiple scattering, and then the author then used a log-normal grain-size distribution.

IV. Scaling Approach to Wavelength and Grain Size Dependence of Ultrasonic Attenuation

A. Introduction to Scaling Approach

The objective of this work is to introduce and apply a novel approach to ultrasonic attenuation based on scaling analysis. Scaling can be defined as a property describing objects or systems that are invariant under certain transformations of scale [Mandelbrot 1983 p. 18]. The discussions in this section demonstrate that power-laws are one appropriate expression for scaling properties. Many research topics involve the study of both the structural and dynamical scaling properties of a system; the research presented here falls into this class of investigation. Fractal concepts are closely associated with scaling because the irregularity or fragmentation for many fractal objects are identical at all scales.

The idea for the scaling work originated with the experimental observation that the wavelength dependence of ultrasound attenuation is an inverse power-law, with a noninteger exponent [Mason & McSkimin 1947, Papadakis 1970, Kumar & Govil 1980]. This is in contrast to the classical derivations in Equation 5, which demand a dependence on an integer (0, 2 or 4) power of the wavelength. Scaling concepts provide an approach to the interpretation of a measurement that exhibits this noninteger power dependence, and can result in the ability to characterize structures or dynamics in terms of straightforward scaling measures that can yield models with a small number of parameters.

Self-similarity is a special kind of scaling, when a piece of an object is geometrically similar to the whole [Mandelbrot 1983 p. 18]. One consequence of self-similarity is that the properties of a self-similar geometric object are indistinguishable as a function of resolution, also known as length scale [Orbach 1986]. No matter how much an image of the object is magnified or reduced, the geometric properties remain the same. This condition is termed 'no characteristic scale.'

Self-similarity may be defined in an exact or statistical sense. The definition for self-similarity above, namely the property that a piece of an object is geometrically similar to the whole, is exact self-similarity. Some applications used the less restrictive definition of statistically self-similarity: the statistical aspects are scale invariant [Sander 1987, Feder 1988 p. 185, Kaye 1989 p. 35]. This work concentrates on statistical self-similarity. It has also been found that some structures in nature may be self-similar over a finite range of length scales [Orbach 1986].

Concepts from scaling theory can be used to justify the consideration of an inverse power-law for the distribution of grain sizes. It is reviewed below that if the size distribution is statistically self-similar, it can be described by an inverse power-law, applicable when there is no characteristic scale for the measurement of the size distribution. To analyze the self-similarity, the scaling argument is applied to two images of grains at different magnifications with finite resolutions: magnification 1, and a higher magnification 2. Figure 2 is provided for illustration purposes:

Histograms can be made at each magnification using $N_1(\partial)$ and $N_2(\partial)$, defined as follows:

$N_1(\partial)\, d\partial$ = number of circles of diameter between ∂ and $d\partial$ at magnification 1

$N_2(\partial)\, d\partial$ = number of circles of diameter between ∂ and $d\partial$ at magnification 2

The question is this: how does the histogram vary as the magnification changes? Unlike the coastline example, a function rather than a single value is generated at each magnification, and an appropriate test for possible scaling relationships must be chosen. The distribution functions are compared at relative positions using the following equation:

$$\frac{N_1(\partial)}{N_1(\partial/b)} \stackrel{?}{=} \frac{N_2(\partial')}{N_2(\partial'/b)} \tag{8}$$

One can think of ∂ as the yardstick, and 'b' as a parameter to make the yardstick smaller (if $b > 1$) or larger (if $b < 1$). If the equality above holds, then $\frac{N(\partial)}{N(\partial/b)}$ is dependent on the parameter 'b' alone, not upon the magnification used. In this example, the circles are termed statistically self-similarly distributed, and there is no characteristic sense of scale for the grain-size distribution. The inverse power-law is the expression of choice to represent such self-similar distributions: $N(\partial) \sim \partial^{-\beta}$. This type of distribution has been observed and discussed in light and x-ray scattering experiments for silica gels [Martin 1986, Martin & Wilcoxon 1988] and for the pore size distribution in lignite coal [Schmidt 1982].

IV.B. Attenuation Coefficient

This section presents a scaling relationship between the ultrasonic attenuation coefficient and the grain-size distribution. As reviewed in Section III, attenuation depends on the wavelength (λ) and the size of the scatterer; the three scattering regions are:

Rayleigh:	$\lambda \gg D$	$\alpha_{\lambda,D}(\lambda,D) = \frac{C_r D^3}{\lambda^4}$
Stochastic:	$\lambda \approx D$	$\alpha_{\lambda,D}(\lambda,D) = \frac{C_s D}{\lambda^2}$
Diffusive:	$\lambda \ll D$	$\alpha_{\lambda,D}(\lambda,D) = \frac{C_d}{D}$

(9)

where D is the diameter or largest length measurement of the grain, and C_r, C_s, and C_d are constants of the material. The notation $\alpha_{\lambda,D}$ is used in this section to underscore the dependence of attenuation on grain size and wavelength. In Equation 11, the attenuation is a function of wavelength alone, and the symbol α_λ is used to reflect this.

The theoretical development begins by defining new functions, called 'scaled attenuations' by multiplying the attenuation by the wavelength [Generazio 1986]:

$$\frac{D}{\lambda} \ll 1 \qquad \lambda\alpha_{\lambda,D}(\lambda,D) = a_{\lambda,D}(\lambda,D) = C_r\left(\frac{D}{\lambda}\right)^3$$

$$\frac{D}{\lambda} \approx 1 \qquad \lambda\alpha_{\lambda,D}(\lambda,D) = a_{\lambda,D}(\lambda,D) = C_s\frac{D}{\lambda}$$

$$\frac{D}{\lambda} \gg 1 \qquad \lambda\alpha_{\lambda,D}(\lambda,D) = a_{\lambda,D}(\lambda,D) = C_d\left(\frac{D}{\lambda}\right)^{-1} \tag{10}$$

The scaled attenuations for these three scattering regions are dependent on the ratio of grain size to wavelength. The theoretical development has been given which results in a single

expression for the attenuation for all wavelengths using the assumption of spherical grains [Roney 1950 p. 14]. Also, the expressions for attenuation in Equation 5 also depend on the ratio of grain size to wavelength for the three scattering regions. It is therefore assumed that the scaled attenuation is always dependent on the ratio of grain size to wavelength, for all ratios of grain size to wavelength.

To account for the distribution of grain sizes, the function N(D) is used, defined as

N(D) dD = the number of grains of size between D and D + dD

Assuming that multiple scattering can be ignored, the scaled attenuation resulting from the distribution of grain sizes is expressed as follows:

$$a_\lambda(\lambda) = \int_0^\infty N(D)\, a_{\lambda,D}(\lambda,D)\, dD \tag{11}$$

The sizes are assumed to be distributed with an inverse power-law with scaling exponent γ:

$$N(D) = KD^{-\gamma},\ 0 < D < \infty$$

$$a_\lambda(\lambda) = \int_0^\infty KD^{-\gamma}\, a(\lambda,D)\, dD \tag{12}$$

One reason for this assumption can be based on statistical self-similarity of the size distribution. Also, as discussed in section II, the cumulative frequency of the grain weight is often represented linearly on the log-log scale [Rhines & Patterson 1982, Doherty 1984], suggesting power-laws may be appropriate models for grain sizes. Lastly, it was pointed out in the same section that the log-normal distribution can be approximated by an inverse power-law for distributions with large variances.

The scaled attenuation functions in Equation 10 are dependent on the ratio $\frac{D}{\lambda}$. This fact will be exploited below, using the notation $a_x(x)$ where $x = \frac{D}{\lambda}$. The change of variables $x = \frac{D}{\lambda}$ in Equation 12 reveals

$$a_\lambda(\lambda) = \int_0^\infty Kx^{-\gamma} \lambda^{-\gamma}\, a_x(x)\, \lambda dx = K\, \lambda^{-(\gamma-1)} \int_0^\infty x^{-\gamma}\, a_x(x)\, dx \tag{13}$$

Since the above inverse power-law relationship between the grain-size distribution and attenuation has not been previously examined, the convergence of the integral in Equation 13 is given below. This results in bounds for the exponent γ. The integral is expressed using different intervals of x:

$$a_\lambda(\lambda) = K\, \lambda^{-(\gamma-1)} \left(\int_0^{x_1} x^{-\gamma}\, a_x(x)\, dx + \int_{x_1}^{x_2} x^{-\gamma}\, a_x(x)\, dx + \int_{x_2}^{\infty} x^{-\gamma}\, a_x(x)\, dx \right) \tag{14}$$

where $x_2 > x_1$ and $x_1 \ll 1$ and $x_2 \gg 1$.

The first integral in Equation 14 tests the convergence for small x. Observing from Equation 10 that

$$a_x(x) \sim x^3, \; x \ll 1$$

the first integral in Equation 14 is

$$x_1 \ll 1 \qquad \int_0^{x_1} x^{-\gamma} x^3 \, dx = \frac{x^{4-\gamma}}{4-\gamma} \Bigg|_0^{x_1} \tag{15}$$

which converges if $4 > \gamma$. Conversely, for large x

$$a_x(x) \sim x^{-1}, \; x \gg 1$$

and the third integral in Equation 14 becomes

$$x_2 \gg 1 \qquad \int_{x_2}^{\infty} x^{-\gamma} x^{-1} \, dx = x^{-\gamma} \Bigg|_{x_2}^{\infty} \tag{16}$$

which converges when $\gamma > 0$. Therefore, the bounds for the scaling exponent are $0 < \gamma < 4$ in order for the integral in Equation 13 to converge. The wavelength dependence of $a_\lambda(\lambda)$ is

$$a_\lambda(\lambda) \sim \lambda^{-(\gamma-1)}, \quad 0 < \gamma < 4 \tag{17}$$

and the expression for the attenuation coefficient becomes

$$\alpha_\lambda(\lambda) = \lambda^{-1} a_\lambda(\lambda) = K \lambda^{-\gamma} \int_0^{\infty} x^{-\gamma} a_x(x) \, dx \; , \; 0 < \gamma < 4 \tag{18}$$

Therefore the exponent for wavelength dependence of attenuation is determined by the exponent for the grain-size distribution. In other words,

the grain-size distribution is an inverse power law with exponent γ	$\Rightarrow$	the dependence of attenuation on wavelength is an inverse power law with exponent γ

It has been proven that the reverse is also true: if the dependence of attenuation on wavelength is an inverse power-law with exponent γ then the grain-size distribution is also an inverse power-law with exponent γ [Nicoletti 1991].

In summary, the work presented in this section proposes a power-law relationship between the proposed grain-size distribution function and the resulting functional dependence of attenuation on wavelength. Additionally, this relationship is shown to be valid if the development starts with the assumption of an inverse power-law for the grain-size distribution or the attenuation. This establishes the first straightforward relationship between the grain-size distribution function and the exponent which characterizes the dependence of attenuation on wavelength, linking the microstructural properties to the dynamical response.

IV.C. Limits of Inverse Power-Law Distribution

This section analyzes the practical limitations of the results shown in section V.B, demonstrating the effect of the choice of wavelength on the measured attenuation exponent. By

using the assumption that an inverse power-law distribution is retained within a limited region ($D_1 < D < D_2$), the expression for the scaled attenuation becomes:

$$a_\lambda(\lambda) = \int_0^{D_1} N(D)\, a_{\lambda,D}(D,\lambda)\, dD + \int_{D_1}^{D_2} KD^{-\gamma}\, a_{\lambda,D}(D,\lambda)\, dD + \int_{D_2}^{\infty} N(D)\, a_{\lambda,D}(D,\lambda)\, dD \tag{19}$$

If the number of grains with size less than D_1 or greater than D_2 is negligible, then the first and third integrals can be assumed to be insignificant in comparison to the second integral and the scaled attenuation can be written as

$$a_\lambda(\lambda) = \int_{D_1}^{D_2} KD^{-\gamma}\, a_{\lambda,D}(D,\lambda)\, dD \tag{20}$$

and after rewriting in terms of $x = \frac{D}{\lambda}$,

$$a_\lambda(\lambda) = \int_{D_1/\lambda}^{D_2/\lambda} Kx^{-\gamma}\lambda^{-\gamma}\, a_x(x)\, \lambda dx = K\lambda^{-(\gamma-1)} \int_{D_1/\lambda}^{D_2/\lambda} x^{-\gamma}\, a_x(x)\, dx \tag{21}$$

Three cases for the ratio of wavelength to D_1 and D_2 are analyzed below:

Case 1:	$\lambda \ll D_1$	(Diffusive scattering only)
Case 2:	$\lambda \gg D_2$	(Rayleigh scattering only)
Case 3:	$D_1 \ll \lambda \ll D_2$	(All three scattering modes simultaneously)

Case 1 ($\lambda \ll D_1$)

If $\lambda \ll D_1$ then the attenuation should be due to diffusive scattering alone and the exponent for the wavelength dependence of the resulting attenuation should be zero (independent of wavelength). From Equation 10

$$x \gg 1 \qquad a_x(x) = \frac{C_d}{x} \tag{22}$$

where $x = \frac{D}{\lambda}$ and the expression in Equation 21 becomes

$$a_\lambda(\lambda) = K\lambda^{-(\gamma-1)} \int_{D_1/\lambda}^{D_2/\lambda} x^{-\gamma} \frac{C_d}{x}\, dx$$

$$= K\, C_d\, \lambda^{-(\gamma-1)} \frac{D_1^{-\gamma} - D_2^{-\gamma}}{\lambda^{-\gamma}} \sim \lambda \tag{23}$$

Thus the attenuation is independent of wavelength, as expected:

$$\alpha_\lambda(\lambda) \sim \lambda^0, \lambda \ll D_1 \tag{24}$$

Case 2 ($\lambda \gg D_2$)

If $\lambda \gg D_2$, then the classical Rayleigh limit should result. In this instance, the expression for the scaled attenuation function reduces to the case in Equation 10 for small x:

$$x \ll 1 \qquad a_x(x) = C_r x^3 \tag{25}$$

resulting in the following dependence of scaled attenuation on wavelength:

$$a_\lambda(\lambda) = K\lambda^{-(\gamma-1)} \int_{D_1/\lambda}^{D_2/\lambda} x^{-\gamma} x^3 \, dx$$

$$= \frac{K\lambda^{-(\gamma-1)}}{4-\gamma}\left(\frac{D_2^{4-\gamma} - D_1^{4-\gamma}}{\lambda^{4-\gamma}}\right) = \frac{K(D_2^{4-\gamma} - D_1^{4-\gamma})}{(4-\gamma)\lambda^3} \tag{26}$$

Thus the exponent for the dependence of attenuation on wavelength is four, as expected:

$$\alpha_\lambda(\lambda) \sim \lambda^{-4}, \lambda \gg D_2 \tag{27}$$

Case 3 ($D_1 \ll \lambda \ll D_2$)

When the range for sizes is very wide ($D_2 \gg D_1$), wavelengths can be carefully selected such that $D_1 \ll \lambda \ll D_2$. For this range of wavelengths all three types of scattering (Rayleigh, stochastic and diffusive) will occur. Also, Equation 21 is consistent with Equation 13 if $\frac{D_1}{\lambda}$ approaches 0 and $\frac{D_2}{\lambda}$ approaches infinity. For this case, the resulting dependence of attenuation coefficient on wavelength is determined by the exponent of the inverse power-law expression for the grain-size distribution, as in section IV.B:

$$\alpha_\lambda(\lambda) = \lambda^{-1} a_\lambda(\lambda) \sim \lambda^{-\gamma}, D_1 \ll \lambda \ll D_2 \tag{28}$$

Therefore, the choice of wavelengths for the ultrasonic experiment is critically dependent on the actual range of grain sizes in the metal sample. If $\lambda \ll D_1$ (Case 1), the measurement of the attenuation should be independent of wavelength (exponent = 0). Conversely if $\lambda \gg D_2$ (Case 2), then the measured attenuation exponent is expected to be four. When $D_1 \ll \lambda \ll D_2$ (Case 3), the measured attenuation exponent is determined by the grain-size distribution exponent. These transitions can be viewed as crossovers from integer to noninteger exponents. The objective of this research effort is the determination of the grain-size distribution exponent, therefore the wavelengths used must be $D_1 \ll \lambda \ll D_2$.

While this work concentrates on nondestructively measuring the grain size exponent, the average grain size is desired for many applications. If the limits of the grain-size distribution as well as the grain size exponent are known, then any statistical moment can be calculated, including the average grain size:

$$\bar{D} = K\frac{D_2^{2-\gamma} - D_1^{2-\gamma}}{2 - \gamma} \tag{29}$$

IV.D. Self-similar Area from Self-similar Volume Distributions

The grain size measurement is conventionally made from a micrograph of the grain structure, an inherently two-dimensional measurement. The notation for the distribution of sizes on the cutting plane is $N_a(\partial)$, where

$$N_a(\partial)\, d\partial = \text{number of circles of size between } \partial \text{ and } \partial + d\partial$$

The relationship between this two-dimensional measurement and the size of the grain (in three-dimensions) will be explored in the following section. If one considers spherical grains*, the relationship between $N_a(\partial)$ and the grain-size distribution in three dimensions, N(D) is [DeHoff 1968 p. 155]

$$N_a(\partial) = \partial \int_{\partial}^{\infty} \frac{N(D)}{\sqrt{D^2 - \partial^2}}\, dD \tag{30}$$

The expression in Equation 30 is known as Abel's Equation [DeHoff 1968 p. 155].

If N(D) is statistically self-similar then the scaling properties provide the following equalities:

$$N(D) = KD^{-\gamma} \qquad N(bD) = a\,N(D)$$

$$\gamma = -\frac{\log a}{\log b} \qquad N(bD) = b^{-\gamma} N(D) \tag{31}$$

If it is assumed that N(D) is statistically self-similar then two questions of interest arise: is $N_a(\partial)$ also self-similar? And if so, with what exponent? To answer these questions, the following renormalization transformation is performed:

$$N_a(k_1\partial) \stackrel{?}{=} k_2 N_a(\partial) \tag{32}$$

for $k_1, k_2 > 0$. Equation 30 is used, and then a change of variables ($D' = D/k_1$) is applied:

$$N_a(k_1\partial) = k_1\partial \int_{\partial}^{\infty} \frac{N(D'k_1)}{\sqrt{g^2D'^2 - k_1^2\partial^2}}\, k_1\, dD' = k_1\partial \int_{\partial}^{\infty} \frac{N(D'k_1)\, dD'}{\sqrt{D'^2 - \partial^2}} \tag{33}$$

From Equation 31,

$$N(D'k_1) = k_1^{-\gamma} N(D') \tag{34}$$

and Equation 33 becomes

$$N_a(k_1\partial) = k_1\partial \int_{\partial}^{\infty} \frac{k_1^{-\gamma} N(D')\, dD'}{\sqrt{D'^2 - \partial^2}} = k_1^{1-\gamma}\partial \int_{\partial}^{\infty} \frac{N(D')\, dD'}{\sqrt{D'^2 - \partial^2}}$$

$$= k_1^{-(\gamma-1)} N_a(\partial) \tag{35}$$

---

* This assumption has been used for nickel grains [Nicholas 1955]

Therefore the exponent for $N_a(\partial)$ is $(\gamma - 1)$ and $N_a(\partial)$ can be written as

$$N_a(\partial) = K' \, \partial^{-(\gamma-1)} \tag{36}$$

This section thus proves that if the grains are self-similarly distributed, then the circles seen on micrograph images of the grain boundaries must also be self-similarly distributed with an exponent one less than the exponent for the volume distribution. This is the first development of its kind, demonstrating the ease of transition of between two and three dimensions for power-law distributions.

As noted in section II, the log-normal distribution has been the only function used by previous researchers to describe the grain-size distribution N(D). The distribution of sizes on the cutting plane from a log-normal distribution of sizes using Abel's Equation is

$$N_a(\partial) = \partial \int_{\partial}^{\infty} \frac{\frac{N_{tot}}{D\sqrt{2\pi\sigma_m^2}} \, e^{-(\ln D - D_m)^2/2\sigma_m^2}}{\sqrt{D^2 - \partial^2}} \, dD \tag{37}$$

where $D_m = E[\ln D]$ and $\sigma_m^2 = E[\ln D^2] - (E[\ln D])^2$. This expression for the two-dimensional size distribution is difficult to evaluate; furthermore, it is clearly not log-normal. Previous work on the relationship between the grain-size distribution and the attenuation neglected this fact [Smith 1982]; the two-dimensional size distribution obtained from the micrograph was fitted with a log-normal curve. Therefore, the assumption of an inverse power-law to describe the three-dimensional grain-size distribution has two important consequences. As developed in section V.B, this assumption results in a simple relationship for the wavelength dependence of attenuation. Furthermore, this section demonstrates that a second outcome of this assumption is a simple relationship between the two- and three-dimensional size distributions.

V. Experimental Design

A. Overview

This section provides a brief overview of the experiments designed to verify the scaling relationship between the grain-size distribution and ultrasonic attenuation as proposed in section V. Two sets of measurements from the same metal sample must be made: 1) the grain-size distribution from the photomicrographs of the grain boundaries, and 2) ultrasonic attenuations. The sample preparation and attenuation measurement set-up take into account the practical constraints of actual grain-size distributions in metal and the desire to obtain precise attenuation measurement.

This set of experiments constitutes the first attempt to establish the proposed scaling relationship between the grain-size distribution and attenuation; therefore, much consideration was given to the use of the simplest material and most precise attenuation measurement possible. Preliminary ultrasonic experiments using stainless steel samples were completed in the Signal Processing Laboratory at Drexel University. The results proved to be unsatisfactory due to diffraction effects dominating the attenuation measurement. The decision was made to use higher frequencies (> 10 MHz) for the ultrasonic measurement and to carefully prepare metal samples to diminish the diffraction as well as reflection coefficient effects. The attenuation and grain-size distribution measurements were made at the Lewis Research Center of the National Aeronautics and Space Administration (NASA), under the supervision of Dr. Edward Generazio. The metal

samples and photomicrographs were sent to the Lewis Research Center, followed by a visit by D. Nicoletti to the facility.

A pure metal rather than an alloy was chosen in order to assure that only grain boundary scattering is occurring. In alloys, such as stainless steel, inclusions can form which will scatter the ultrasonic wave differently than the grains. Nickel was chosen because of its inexpensiveness and ready availability in commercially pure form (99.6 per cent pure).

The metal processing steps include rolling and annealing. To satisfy the arguments in section V.C, these processing steps should result in a grain-size distribution that is as wide as possible. The size distribution should also be spatially homogeneous, and any anisotropy in the shape of the grains should be minimized.

The grain-size distribution was measured using photomicrographs of the grain boundaries, as discussed in section II. Therefore one step of the sample preparation was the necessary polishing and etching of the surface to emphasize the grain boundaries, which were recorded using photomicrographs. A final polishing prepared the metal surface for the precision attenuation measurement.

The attenuation measurement was designed to balance the constraints of diffraction, significant for large wavelengths, and large attenuation (> 5 Np/cm), significant for small wavelengths. Large attenuation causes the energy of the echoes to be scattered to the extent that their measurement is overpowered by the noise level, and is significant for small wavelengths because attenuation is inversely proportional to wavelength. For some wavelength ranges and material preparations, the reflection coefficient is wavelength dependent. Rather than assume independence of wavelength, the reflection coefficient was measured and corrected for to eliminate its contribution to the attenuation measurement.

V.B. Sample Preparation

This section details the material processing steps as well as the photomicrographic techniques. The final result is three nickel samples with different annealing durations. Nine photomicrographs of the three samples form the data set used for the grain-size distribution measurement (twenty-seven micrographs in total).

Nickel 200 samples were obtained from Inco Alloys International, Huntington, West Virginia. Nickel 200 is commercially pure (99.6%) wrought nickel, with the following maximum percentage chemical composition:

Copper:	0.25	Iron:	0.04
Manganese:	0.35	Carbon:	0.15
Silicon:	0.35	Sulfur:	0.01

The structure of nickel is face-centered cubic. Commercial uses for Nickel 200 include the manufacture of a variety of processing equipment, particularly to maintain product purity in handling foods, synthetic fibers, and alkalies.

The final samples should have a homogeneous distribution of grain sizes, ideally with an isotropic configuration to satisfy the arguments used in the theoretical development in section V.C. The processes of cold working, recrystallization, and grain growth were used to achieve the desired product.

Cold work was achieved in this application by rolling the nickel. The processing steps for the nickel must take into account the three steps of annealing: recovery, recrystallization, and grain growth. For the desired metal samples, the recovery stage should be complete and the process of recrystallization should begin, and the grain growth must be limited in order that the distribution of the grain size will contain very small as well as large grains. Six factors influence recrystallization:

amount of prior deformation, temperature, time, initial grain size, composition, and amount of recovery prior to the start of recrystallization [Dieter 1961 p. 155]; therefore different annealing durations will be tested to achieve the desired structure.

There were three additional steps used for the sample preparation: 1) the final samples used for ultrasonic attenuation measurement must be less than .10 inch thick, flat and parallel to within ± $\frac{1}{2}$ mil, 2) photomicrographs of the grain boundaries are required, and 3) the final sample must be polished on one side to a mirror finish.

All processing steps were completed in the Metallographic Laboratory of the Materials Engineering Department of Drexel University. The original nickel plate was approximately 6 x 5 x $\frac{1}{8}$ inches, and was initially annealed and rolled by Inco Alloys. An analysis was completed on the nickel, using polishing and etching to bring out the grain boundaries. The photomicrographs showed that the grains were deformed from Inco's processing steps. It was therefore determined that an additional rolling and annealing process was necessary to allow recrystallization to occur, resulting in the grain shape and size distributions desired. The nickel was cut into 1-inch wide strips, and then the rolling was done on a 2 roll Stanat mill. Unidirectional rolling was used while the nickel strip was fed in for each pass, reversing sides each time to minimize warpage. Rolling reduction per pass were approximately 10 mils, accumulating in a final reduction of 50%.

The rolled strip was cut into approximately 1 x 1 inch tiles on a slow speed band saw. The samples were then mechanically ground to within ±1/2 mil tolerance for parallel tile faces.

The tiles were first used to establish the annealing times needed to cause recrystallization to occur. One sample was annealed at 800 °C for 1 minute; the steps for the anneal began with opening the furnace door, and the samples were placed on a steel tray which was at temperature (800 °C). Dwell times (in this case, 1 minute) began once furnace door closed. The thermocouple reading of furnace atmosphere dropped to about 720 - 730 °C while the furnace door was open. The steel tray was used to minimize heat loss upon opening oven doors. The samples were air cooled on insulating, room temperature ceramic blocks.

After polishing, etching 50/50 nitric/glacial acetic acid mixture, and making a micrograph, it was clear that the recovery stage of annealing had not been completed and recrystallization had not begun. The other two tiles were annealed for 2 and 5 minutes, and the micrographs showed that the grain sizes desired is achieved for these annealing durations. Thus the three remaining tiles not yet processed were annealed for 2, 3 and 5 minutes.

The next step was to obtain high quality micrographs of the grain boundaries of the final three tiles. To achieve this, the samples were ground on 120 - 280 - 320 - 400 - 600 grit papers in order to remove previous grit paper's deformation layers. They were then polished on a canvas cloth impregnated with 9 micron diamond slurry, followed by a 0.3 micron alumina polish on a Selvyt cloth.

To bring out the grain boundaries, the samples were immersion etched for 40 - 45 seconds in a 50/50 nitric/glacial acetic acid mixture. The alumina polish-etch cycle was repeated four more times to remove as much grinding-induced deformation as possible.

After the final etch, photographs were taken on a Zeiss ICM 405 Metallograph. 33 photographs in total were taken: 11 at each annealing time, 9 at 100x for analysis and one each at 32x and 200x. The nine micrographs at 100x were used for grain-size distribution measurement at the Lewis Research Center of the National Aeronautics and Space Administration (NASA); the image processing technique is described in section II. A final alumina polishing was done to remove the etched surface and create a mirror finish. The final thicknesses were measured using a micrometer to be 0.1309, 0.1299 and 0.1279 centimeters for the two-, three- and five-minute samples, respectively.

After the ultrasonic measurements were complete, additional photomicrographs were made on the side surfaces of the sample. These additional micrographs were taken to establish if the grains are equiaxed.

V.C. Attenuation Measurement

For metals, the standard method of attenuation measurement involves the transmission of a pulse of ultrasonic energy into the sample, followed by the recording of multiple echoes of the pulse as it travels across the specimen and is reflected at the edges of the material. Fourier transforms of these echoes allow the computation of the attenuation for a range of frequencies.

Attenuation measurements reported here were made at the Lewis Research Center of the National Aeronautics and Space Administration (NASA). The equipment used for these measurements is very similar to the equipment used for the preliminary ultrasonic experiments using stainless steel samples, which were completed in the Signal Processing Laboratory at Drexel University. Therefore, it is possible to make the attenuation measurements in the Signal Processing Laboratory. However, since it was necessary to make the grain-size distribution measurements at the Lewis Research Center, the decision was made to complete the ultrasonic analysis there as well, with a site visit by D. Nicoletti.

Two major obstacles to accurate ultrasonic attenuation measurements are diffraction and reflection coefficient effects, as well as the need for the attenuation to be small enough to allow accurate ultrasonic recordings. The experimental design presented below strikes a balance among these considerations.

The samples are very thin (less than .15 centimeters thick) when compared to metal samples used in other attenuation measurements. For comparison, previous researchers have used 1 cm [Smith et. al. 1981], 1.9 cm [Papadakis 1963], 0.63 to 2.9 cm [Klinman & Stephenson 1981]. A 30 MHz center frequency transducer was used. The attenuation measurement scheme for pulse-echo, contact mode [Generazio 1985], is shown in Figure 3.

A quartz buffer rod and glycerin couplant are used between the piezo-electric crystal and the specimen. Each echo (FS_1, FS_2, B_1, and B_2) was obtained by performing 64 time averages. The echoes were first recorded without the sample: FS_1, from the front surface of the buffer rod. Once the transducer was in contact with the specimen, the echo was again recorded from the front surface of the buffer rod, labeled FS_2. Thus the frequency dependent buffer-couplant-sample, R(f), can be obtained using the magnitudes of Fourier transforms of FS_1 and FS_2:

$$|R(f)| = \frac{|FS_2(f)|}{|FS_1(f)|} \tag{38}$$

$FS_1(f)$ and $FS_2(f)$ indicate the magnitude spectra of FS_1 and FS_2, calculated using a Fast Fourier Transform (FFT). With the transducer still in contact with the specimen, the first and second echoes from within the specimen, B_1 and B_2, were recorded. The magnitude of the Fourier transforms of these echoes can be expressed as

$$|B_1(f)| = |FS_1(f)|\,(1 - |R(f)|^2)\exp\{-2\,\alpha(f)\,d\}$$

$$|B_2(f)| = |FS_1(f)|\,(1 - |R(f)|^2)\,|R(f)|\exp\{-4\,\alpha(f)\,d\} \tag{39}$$

where d is the thickness of the sample.

The attenuation can be found from these four measurements:

$$\alpha(f) = \frac{1}{2d}\ln\left(\frac{|B_1(f)|\,|R(f)|}{|B_2(f)|}\right) \tag{40}$$

where ln() denotes the natural logarithm function. The resulting units for the attenuation is Nepers per centimeter (Np/cm).

Piezoelectric transducers are in general inherently band-limited devices, therefore the usable range of frequencies (or wavelengths) for the measured attenuation must be chosen. The frequency range for the above measured attenuation is a result of the FFT calculations, and is a set of discrete points from 0 Hz to half the sampling rate (2.56 GHz). An upper limit for the attenuation should be set to assure that the measured echoes are not attenuated to the extent that their measurement is overpowered by the noise level. An upper limit of 5 Np/cm was chosen. For this value of attenuation, given a sample thicknesses of 0.12 cm, the amplitude of the second echo is $e^{-5*3*.12}$ or 0.016 times the input amplitude. Since attenuation is inversely related to wavelength (Equation 9), an upper limit of 5 Np/cm gives the lower limit for the wavelength range. Other criteria can be used for the choice of the usable range of wavelengths, including the 3 dB or 6 dB bandwidth of the transducer, or consideration of the experimental uncertainty associated with high attenuation ultrasonic measurement.

The attenuation theoretically should decrease or remain constant with increasing wavelength. The upper limit for the wavelength, λ_N, will be chosen to include the attenuation curve up to the point it starts to increase with wavelength; i.e., if $\alpha(\lambda_{i+1}) > \alpha(\lambda_i)$ then $i = N$ and $\alpha(\lambda_i)$ is the last value used in the presented attenuation measurement. The upper and lower limits are expected to be change from sample to sample. However, in order to compare the attenuation curves for all three samples, the values for the lower and upper limit for the wavelengths are chosen using the attenuation measured for the two-minute sample.

VI. Experimental Results

A. Grain-Size Distribution

1. Experimental Results

The experimental results of the grain-size distribution measurement are presented in this section. The isotropy of the distribution is investigated, and the mean and variance of the distributions are calculated. The inverse power-law approximation is displayed and statistically analyzed.

The log-normal distribution has been previously used to describe the grain-size distribution in three-dimensions. It is worth repeating that a log-normal distribution in three-dimensions does not imply that the distribution in two-dimensions is also log-normal. The two-dimensional representation of the grains from the micrographs are used in this work for the size distribution measurement. Therefore, it is inappropriate to compare the log-normal fit of the data to the inverse power-law fit since testing the appropriateness of the log-normal fit in two-dimensions has no bearing on a possible log-normal fit of the three-dimensional grain-size distribution.

The grain-size distribution was measured at the NASA Lewis Research Center from nine photomicrographs of each sample, using the tone-pulse-encoded technique described in section II. Using the notation from section IV.C, the histograms are a measurement of $N_a(\partial)$, defined as

$$N_a(\partial)\, d\partial = \text{number of grains of size between } \partial \text{ and } \partial + d\partial$$

These histograms are shown for the three samples in Figure 4a. Each histogram consists of 256 data points; the 67 non-zero points ($N_a(\partial) \neq 0.0$) are used for the figure. As discussed in section II, the algorithm used for the grain-size distribution measurement has a lower limit for the resolution of small grains due to the need for at least ten pixels to encode a three-cycle sine wave. This lower limit explains the abrupt cut-off of the grain-size distributions for small grain sizes.

The average grain size can be computed from the histogram as follows:

$$\text{average} = E[\partial] = = \frac{\sum_{i=0}^{255} \partial_i N_a(\partial_i)}{\sum_{i=0}^{255} N_a(\partial_i)} \tag{41}$$

and are as follows:

	Average
Two-minute sample:	88.0 microns
Three-minute sample:	90.8 microns
Five-minute sample:	96.7 microns

As expected, the average grain size grows with increased annealing time, also seen by a relative comparison of the histograms in Figure 4a.

The grain-size distributions and averages are very close for the three samples - the average grain sizes differ by as little as 3.2 per cent. This is desirable due to the wavelength considerations in the attenuation measurement. In order to measure the grain size exponent, the wavelength used must be within the range of the grain sizes. Also, in general transducers inherently have finite bandwidths. Therefore, if samples were prepared with very different grain size ranges, it would not be possible to use a single transducer for the ultrasonic measurements. The alternative is to use multiple transducers with different center frequencies, introducing the problem of comparing measurements from different transducers.

VI.A.2. Inverse Power-Law Approximation

The results of the experiment designed to test the hypothesis presented in section IV.B are presented below, namely whether a power-law dependence is a suitable model for the grain-size distribution. The histograms are presented on a log-log scale in Figure 4b. Except for the small number (five) of assumably anomalous points at the beginning and end of the histograms, a the power-law approximation seems appropriate.

There are two possible explanations for these five points in question. As discussed in section IV.C, the inverse power-law can be valid over a finite range of sizes only. Therefore, one explanation for these five points is that they lie outside of the region described by the inverse power-law, $[D_1, D_2]$. For this case, the exponent for the wavelength dependence of the attenuation is determined by the grain-size distribution exponent as long as the inverse power-law dominates the overall size distribution. A second possible explanation comes from a property of the algorithm used to calculate the size distribution. As mentioned in section II, the grain size measurement for the smaller grains is expected to have a high degree of uncertainty than the measurement for the larger grains. Thus, the difference between the measurement for the three points at the beginning of the curves and the power-law approximation may be due to this algorithm-based error.

The mean-square-error (MSE) and correlation coefficient are used for a quantitative judgement. These statistical measurements were applied to the entire data set. For comparison, calculations were also made for the set excluding the three points at the beginning and the two points at the end of the curve; this subset of the data points is labeled "partial data set" below.

The grain-size distributions measurements with the lines indicating the linear approximations based on the entire data set are shown in Figure 5a, 6a and 7a for the two-, three- and five-minute samples, respectively. Linear regression was used to calculated the slope and y-

intercepts. For comparison, the linear approximations based on the partial data set are presented in Figure 5b, 6b and 7b for the two-, three- and five-minute samples, respectively.

Entire data set:

Grain size range: $10^{1.29}$ to $10^{2.44}$ (19.5 to 277) microns

	slope	y-intercept	power-law expression
Two-minute sample:	-1.24	4.15	$Na(\partial) = 14{,}200\ \partial^{-1.24}$
Three-minute sample:	-1.18	4.07	$Na(\partial) = 11{,}700\ \partial^{-1.18}$
Five-minute sample:	-1.04	3.88	$Na(\partial) = 7{,}640\ \partial^{-1.04}$

Partial data set:

Grain size range: $10^{1.49}$ to $10^{2.43}$ (31.2 to 269) microns

	slope	y-intercept	power-law expression
Two-minute sample:	-1.45	4.63	$Na(\partial) = 42{,}900\ \partial^{-1.45}$
Three-minute sample:	-1.38	4.54	$Na(\partial) = 34{,}600\ \partial^{-1.38}$
Five-minute sample:	-1.22	4.30	$Na(\partial) = 20{,}100\ \partial^{-1.22}$

To measure the appropriateness of the linear relationship for the log-log representation of the attenuation data, the sample correlation coefficient **r** was computed:

Entire data set:

Grain size range: $10^{1.29}$ to $10^{2.44}$ (19.5 to 277) microns

	r	r^2
Two-minute sample:	-0.925	85.6%
Three-minute sample:	-0.918	84.3%
Five-minute sample:	-0.894	80.0%

Partial data set:

Grain size range: $10^{1.49}$ to $10^{2.43}$ (31.2 to 269) microns

	r	r^2
Two-minute sample:	-0.994	98.7%
Three-minute sample:	-0.989	97.9%
Five-minute sample:	-0.988	97.5%

The negative sign for the sample correlation coefficient is due to the negative slope. This statistical measurement shows that over 97% of the variations in the values of log(distribution) are accounted for by a linear dependence on log(size) for the partial data set.

A second method of measuring the closeness of the linear fit is through the mean square error (MSE) and root mean square error (RMSE). The results are:

Entire data set:

Grain size range: $10^{1.29}$ to $10^{2.44}$ (19.5 to 277) microns

	MSE	RMSE
Two-minute sample:	0.00157	0.0397
Three-minute sample:	0.00156	0.0505
Five-minute sample:	0.00235	0.0485

Partial data set:

Grain size range: $10^{1.49}$ to $10^{2.43}$ (31.2 to 269) microns

	MSE	RMSE
Two-minute sample:	0.00170	0.0412
Three-minute sample:	0.00255	0.0505
Five-minute sample:	0.00235	0.0485

As outlined in section IV.A, self-similar distributions are invariant to magnification. In an attempt to demonstrate this for the grain-size distributions, the photomicrographs were magnified using a photocopier. The results were unsatisfactory because the distribution is approximately 1.2 decades wide, a range not broad enough to allow self-similarity analysis over many magnifications. Therefore the appropriateness of the inverse power-law for the grain-size distribution was judged using the measured histograms alone.

VI.B. Attenuation Measurement

1. Experimental Results

The attenuation experiments were carried out at the NASA Lewis Research Center. Measurements were made from different transducer locations for each sample: six locations for the two-minute, three locations for the three-minute, and four locations for the five-minute samples. The choice for the number of locations for each samples was arbitrary; more measurements were made for the two-minute sample since it was the first sample used for the ultrasound attenuation experiment. The averaged 44-point curves are shown in Figure 8 for the three samples, for both the linear-linear and log-log axes. The curves are approximately linear on the log-log scale, indicating that a power-law dependence on wavelength is an appropriate model for attenuation.

Before the attenuation exponent is presented, it is interesting to note in Figure 8b that there is a "knee" in the data presented at approximately $10^{2.4}$ or 250 microns. This observation is explained by comparing the grain size and wavelength ranges. The limits for grain size are $10^{1.3}$ and $10^{2.4}$ (20 and 250) microns, while the wavelength range from $10^{2.1}$ to $10^{2.5}$ (125 - 310) microns. As discussed in section IV.C, the wavelength must be between the largest and smallest grain size in order to measure the size distribution's exponent. Thus, the wavelengths are equal to or greater than the largest grain size for the region $\lambda = 10^{2.4}$ to $10^{2.5}$ (250 to 310) microns, and the change in slope is believed to be simply the result of this fact. As the wavelength becomes much greater than the largest grain size, a crossover occurs and the exponent should approach 4, the theoretical limit for Rayleigh scattering.

One further piece of information that can be extracted from the attenuation curves is the following: for which sample is the corner more pronounced? This is answered theoretically by

deciding which sample is dominated more by Rayleigh scattering for the upper region of the curve, i.e. for the wavelength range of $10^{2.4}$ to $10^{2.5}$ (250 to 310) microns. Because of the relative shapes for the histograms (Figure 4), the wavelengths for this region will be greater than a larger percentage of the entire number of grains for the two-minute sample than it is for the three- and five-minute samples. It is, therefore, anticipated that the corner will be more pronounced for the two-minute sample; this is also exhibited in Figure 8.

VI.B.2. Inverse Power-Law Approximation

The exponents were computed for the wavelength range up to $10^{2.4}$ or 250 microns using linear regression to find the slope. The attenuation measurements with the lines indicating the linear approximations are shown in Figures 9, 10, and 11 for the two-, three-, and five-minute samples, respectively. A line with a slope of -4 is drawn for the range $10^{2.4}$ to $10^{2.5}$ (250 to 310) microns to show that the exponent is approaching the Rayleigh scattering exponent (4).

Below is a table for the computed slopes and y-intercepts for the data points from the wavelength region up to $10^{2.4}$ or 250 microns:

	slope	y-intercept	power-law expression
Two minute sample:	-2.401	5.6937	$\alpha(\lambda) = 493{,}969\,\lambda^{-2.401}$
Three minute sample:	-2.339	5.6253	$\alpha(\lambda) = 421{,}988\,\lambda^{-2.339}$
Five minute sample:	-2.338	5.7078	$\alpha(\lambda) = 510{,}270\,\lambda^{-2.338}$

These values for the exponent are clearly within the range previously measured for Nickel 200 samples using very similar preparation: 1.6 to 2.6 [Generazio 1988c]. The exponents decrease (slightly) as the annealing duration increases, also seen in the results reported in Generazio 1988c.

Error bars are provided in Figures 9, 10, and 11 for selected data points. The experimental error was computed as follows. The standard deviation (σ) was found for the linear-linear representations of the attenuation curves for each wavelength. Therefore on the linear-linear scale, the average attenuation has an experimental uncertainty of $\pm\,\sigma$. To represent the error on the log-log scale, the error bar was defined as follows. For a given attenuation value of $\alpha(\lambda)$, the error bar was computed as either $\{\log(\alpha(\lambda)+\sigma)-\log(\alpha(\lambda))\}$ or $\{\log(\alpha(\lambda)-\sigma)-\log(\alpha(\lambda))\}$, whichever was larger in magnitude.

To measure the appropriateness of the linear relationship for the log-log representation of the attenuation data, the sample correlation coefficient r was computed using the wavelength range up to $10^{2.4}$ or 250 microns:

	r	r^2
Two minute sample:	-0.9989	99.77%
Three minute sample:	-0.9987	99.75%
Five minute sample:	-0.9988	99.76%

The negative sign for the sample correlation coefficient is due to the negative slope. This statistical measurement shows that over 99.7% of the variations in the values of log(attenuation) are accounted for by a linear dependence on log(wavelength).

Similar to the analysis for the grain-size distributions, second method of measuring the closeness of the linear fit of the log-log attenuation curves is through the mean square error (MSE) and root mean square error (RMSE); the results are:

	MSE	RMSE
Two-minute sample:	0.0001021	0.01010
Three-minute sample:	0.0001053	0.01026
Five-minute sample:	0.0001024	0.01012

VI.C. Comparison of Grain Size and Attenuation Exponents

A direct superposition of the log-log representations of the grain-size distribution measurements and the attenuation measurements to test this hypothesis is not possible for two reasons. First, as mentioned in section IV.D the ultrasonic attenuation measurement is performed in three dimensions, while grain-size distribution is extracted from a two-dimensional photomicrograph. The exponent for the attenuation must be reduced to the lower dimension by subtracting one before comparing it to the grain-size distribution. This correction factor could be made using the following logic: if a line is described as

$$y = mx + b \tag{42}$$

then a second line, y', with a slope of (m - 1) can be drawn using

$$y' = (m-1)x + b = mx + b - x = y - x \tag{43}$$

Thus, the attenuation measurement, $\alpha(\lambda)$, could be corrected by plotting $(\log\{\alpha(\lambda)\} - \log\lambda)$ versus $\log\lambda$; the slope of this curve is one less than the slope of $\log\{\alpha(\lambda)\}$ versus $\log\lambda$. However, this leads to the second reason for not juxtaposing the two measurements: the ranges of wavelength and grain size are not similar enough to make the graphs meaningful.

Since the ultrasonic measurement was intended as a nondestructive method of measuring the grain-size distribution, the exponent for the attenuation was computed for the wavelength range of $10^{2.1}$ to $10^{2.4}$ (125 to 250) microns, reduced by one, and then lines with this slope were superimposed on the log-log representations of the grain-size distribution. The y-intercept of these lines were computed using the slope predicted from the attenuation measurement and the histogram data points, using both the entire set of data as well as the set excluding the three points at the beginning and the two points at the end of the curve. The mean square error is used as the criterion for judging the appropriateness of using the attenuation exponent as a measurement of slope of the grain-size distribution; if it is, then the hypothesis that the exponents for the attenuation and grain-size distribution are identical is validated.

The exponent computed from the attenuation curve for the two-minute sample is -2.401. A line with a slope of -(2.401 - 1) = -1.401 is shown superimposed on the grain-size distribution in Figure 12. Similarly, lines with slopes of -1.339 and -1.338 are drawn over the grain-size distributions for the three- and five-minute samples in Figures 13 and 14, respectively.

The closeness of the linear fit is based on the mean square error (MSE). The MSE values were computed for the grain size histogram using the slope predicted by the attenuation exponent. These statistical measurements are applied to the entire data set. For comparison, calculations are also made for the set excluding the three points at the beginning and the two points at the end of the curve; this subset of the data points is labeled "partial data set" below.

Entire data set:

Grain size range: $10^{1.29}$ to $10^{2.44}$ (19.5 to 277) microns

	MSE	RMSE
Two-minute sample:	0.0256	0.160
Three-minute sample:	0.0256	0.160
Five-minute sample:	0.0325	0.180

Partial data set:

Grain size range: $10^{1.49}$ to $10^{2.43}$ (31.2 to 269) microns

	MSE	RMSE
Two-minute sample:	0.00184	0.0429
Three-minute sample:	0.00268	0.0517
Five-minute sample:	0.00318	0.0564

Theoretically, the entire size distribution should be linear with a slope equal to the attenuation exponent minus one; the upper portions of the curve in Figure 12 and 14 appear to be better fits. To demonstrate this quantitatively, the MSE and RMSE calculations were made as above except the lower limit range of grain sizes used in the calculations is changed to $10^{2.006}$ or 102 microns. These values are:

Grain size range: $10^{2.01}$ to $10^{2.43}$ (102 to 269) microns

	MSE	RMSE
Two-minute sample:	0.00167	0.0409
Three-minute sample:	0.00288	0.0537
Five-minute sample:	0.00169	0.0411

The fact that the upper portion of the curve is a better fit (for the two- and five-minute samples) is not a discouraging sign for two reasons. First of all, the upper portion contains a larger percent of the total data points because the grain size histogram was originally generated on the linear scale and then represented on the logarithmic scale. Secondly, as discussed in section II, the algorithm used to measure the size distribution is more accurate for the larger grain sizes [Generazio 1988b]. Therefore, the hypothesis that the attenuation exponent is a valid and nondestructive measurement of the exponent for the grain-size distribution is validated with this experimental evidence.

VI.D. Scaling Relationships for Annealing Times

This section examines the scaling of both the grain-size distribution and ultrasonic attenuation as the annealing time increases. If one inspects the effect of the annealing time on the size distribution (Figure 4), it appears that the curves simply shift upwards with increased annealing time, and the shape of the distribution does not change dramatically.

This observation is reinforced by a metallurgical process known as normal grain growth [Atkinson 1988]. This type of growth is observed in a wide variety of materials, and has two properties: 1) a relatively narrow range of grain sizes and shapes, and 2) a time-invariant distribution of sizes. In other words, as grain growth proceeds with increased annealing time, the

form of the distribution is preserved. These two properties are exhibited in the size distributions measured from the nickel samples used in this study.

This section assumes that the size distribution simply scales as the annealing time grows. This approach was also examined in Generazio 1986, using an average grain size measurement instead of the grain-size distribution. Thus basis curves could be formed from the known attenuation and grain-size distribution for *one* sample (either a priori or through a destructive measurement), then the size distributions for other samples could be found by making relative, scaling measurements of the attenuation. The attenuation and grain-size distribution measurements for the two-minute sample comprise the basis curves, and the three- and five-minute curves are approximated below by making the appropriate shifts.

If $N_i(D)$ is the histogram for the i-th minute sample (i=2, 3 or 5), then this scaling can be represented with inverse power-law with identical exponents:

$$N_2(D) = K_2 D^{-\gamma}; \qquad N_3(D) = K_3 D^{-\gamma}; \qquad N_5(D) = K_5 D^{-\gamma} \tag{44}$$

The slopes of the log-log representations of these functions will in theory be identical for all three samples, and equal to - γ. $N_2(D)$ can be shifted by $\{\log(K_3) - \log(K_2)\}$ to form $N_3(D)$. Similarly, $N_5(D)$ is constructed by shifting $N_2(D)$ by $\{\log(K_5) - \log(K_2)\}$.

It has been proven [Nicoletti 1991] that the shifts for the distribution of circles on the cutting plane are identical to the shifts for the distribution of spheres in a volume. $N_{a;2}(\partial)$ is shifted by $\log(K_3) - \log(K_2)$ to obtain $N_{a;3}(\partial)$, and similarly $N_{a;5}(\partial)$ is the result of shifting $N_{a;2}(\partial)$ by $\log(K_5) - \log(K_2)$.

Equation 18 gives the following expression for the attenuation:

$$\alpha(\lambda) = K \lambda^{-\gamma} \int_0^\infty x^{-\gamma} a(x)\, dx \tag{45}$$

with a grain-size distribution equal to $KD^{-\gamma}$. Using the expressions for the grain-size distribution in Equation 44, the three attenuation functions are

$$\alpha_2(\lambda) = K_2 \lambda^{-\gamma} \int_0^\infty x^{-\gamma} a(x)\, dx$$

$$\alpha_3(\lambda) = K_3 \lambda^{-\gamma} \int_0^\infty x^{-\gamma} a(x)\, dx$$

$$\alpha_5(\lambda) = K_5 \lambda^{-\gamma} \int_0^\infty x^{-\gamma} a(x)\, dx \tag{46}$$

for the two-, three- and five- minute samples, respectively. Thus the shifts for the log-log representations of the attenuation measurements are $\{\log(K_3) - \log(K_2)\}$ and $\{\log(K_5) - \log(K_2)\}$, the same shifts used for the grain-size distributions. Therefore, if the size distribution exponent (and therefore the attenuation exponent) remains constant for different annealing times, then the measured shift in the log-log attenuation curve corresponds to the shift or

scaling of the grain-size distribution as well. The attenuation measurements resulted in the following parameters:

	exponent (slope)	log(K) (y-intercept)
Two minute sample:	-2.401	5.6937
Three minute sample:	-2.339	5.6253
Five minute sample:	-2.338	5.7078

The exponents (-2.401, -2.339 and -2.338) are very close; the maximum percent change is only 2.7%. There is a problem though when the y-intercepts are compared for the two- and three-minute samples. The three-minute curve is higher than the two-minute curve, yet the y-intercept computed is smaller for the three-minute curve. This is a result of the lines found from linear regression intersecting *outside of the range of the measurement*, forcing $\log(K_2)$ to be larger than $\log(K_3)$. Since this does not represent the observation that the measured three-minute curve is an upward-shifted version of the measured two-minute curve, the following correction was made. The attenuation curves presented in Figure 8 were translated to the left by 2.097, creating the following new curves:

$$\alpha_i^*(\lambda) = \alpha_i(\lambda - 2.097),\ i = 2, 3, 5 \tag{47}$$

The slopes computed using linear regression on $\alpha_i^*(\lambda)$ are identical to the slopes from $\alpha_i(\lambda)$; the y-intercept will change, as follows:

	exponent (slope)	$\log(K^*)$ (y-intercept)	$\log(K^*) - \log(K_2^*)$
$\alpha_2^*(\lambda)$:	-2.401	0.65905	----
$\alpha_3^*(\lambda)$:	-2.339	0.72032	0.06127
$\alpha_5^*(\lambda)$:	-2.338	0.80570	0.14665

These y-intercept values correctly reflect that the curves shift up as the annealing duration increases. The values given above for $\log(K^*) - \log(K_2^*)$ replace the shift values given previously.

Figure 15 shows the results of shifting $\alpha_2(\lambda)$ by 0.06127 to estimate $\alpha_3(\lambda)$, and similarly, shifting $\alpha_2(D)$ by 0.14665 is drawn as a representation of $\alpha_5(\lambda)$ in Figure 16. It is clear that the shapes of the curves are close enough to allow a simple shift to obtain one curve from another.

The hypothesis that the shifts for the attenuation measurement curves are equivalent to the shift for the grain-size distribution curves is tested next. $N_2(D)$ is shifted by 0.06127 and 0.14665 in Figures 17 and 18 to estimate $N_3(D)$ and $N_5(D)$, respectively.

The agreement between of the shifted curves and the measured histograms has two important ramifications: first, it is further experimental evidence of the proposed scaling relationships between attenuation and grain-size distribution. It also suggests an important nondestructive evaluation technique, described as follows. Assuming that the exponent is the same for a series of metal samples and that the grain-size distribution is known for *one* sample (either a priori or through a destructive measurement), then the size distributions for all of the other samples could be found by measuring the shifts of the attenuation curves.

VII. Conclusions and Future Directions

This research deals with the application of nondestructive ultrasonic testing to grain-size distribution measurement in metals. A novel scaling relationship between ultrasonic attenuation and grain-size distribution is developed, demonstrating how the complex structure of the grain boundaries can be analyzed using the measured ultrasonic attenuation. It has been pointed out that researchers have often made two assumptions: 1) Rayleigh scattering dominates, and 2) the grain-size distribution can be represented by a single value, the average grain size. The result of these assumptions has been the use of the following expression for attenuation:

$$\alpha(f) \sim \left(\overline{D}\right)^3 f^4 \tag{48}$$

This relationship has two serious shortcomings for many experimental results, both of which are consequences of the grain-size distribution. First, the assumption that the attenuation is dominated by Rayleigh scattering requires that the wavelength is much greater than the scatterer size. Since the largest grain size may be significantly larger than the average grain size, wavelengths chosen based on the average grain size may in fact be comparable to the largest grain size. Secondly, dependence on the third power of the average grain size as an accurate grain volume relationship may not be valid if there is a distribution of grain sizes. If a distribution exists, then the third moment must be used, which in general is not equal to the cube of the first moment (or average).

The literature survey in section III shows that the only expression previously used for a grain-size distribution function is the log-normal. The first contribution to an alternative theoretical development for attenuation is to use an inverse power-law for the grain-size distribution. Justification for this representation of the size distribution can be found when scaling theory is applied to micrographs of the grain boundaries, as demonstrated in section IV, as well as the linearity of the cumulative frequency of the grain weight on the log-log scale [Rhines & Patterson 1982, Doherty 1984].

The evolution of this theoretical work continues to unfold by showing that if the grain-size distribution is an inverse power-law, then the wavelength dependence of attenuation is also an inverse power-law, with the same exponent as the grain-size distribution. Careful attention is given to the limitations of the new scaling theory in terms of a practical grain-size distribution with a finite upper size limit. Thus, a novel method is presented relating the attenuation exponent to the grain-size distribution.

The dependence of the measured attenuation exponent on the relative size of the wavelength to the finite grain size range is explored in section IV.C. If the experimentally measured attenuation exponent is four, then the wavelength is interpreted to be much greater than the largest grain size, and the expression for the attenuation becomes

$$\alpha(\lambda) \approx \frac{K(D_2^{4-\gamma} - D_1^{4-\gamma})}{(4-\gamma)\lambda^4} \qquad \lambda \gg D_2 \tag{49}$$

Conversely if $\lambda \ll D_1$, then the measured attenuation exponent is expected to be zero:

$$\alpha(\lambda) \approx K\, C_d (D_1^{-\gamma} - D_2^{-\gamma}) \qquad \lambda \ll D_1 \tag{50}$$

For exponent values between zero and four, the wavelength must be between the smallest and largest grain size, and the attenuation exponent can be directly related to the grain-size distribution exponent.

One of the most significant contributions of this work is for attenuation measured using this range of the relative values of wavelength and grain size ($D_1 \ll \lambda \ll D_2$). If Rayleigh scattering dominates, then the dependence on the fourth power of wavelength can be used. After choosing

an appropriate expression for the grain-size distribution, the resulting attenuation can be evaluated. Thus the inverse power-law expression for the grain-size distribution does not improve the understanding of the effect of the size distribution on the attenuation for this type of scattering. However, when the wavelength is between the largest and smallest grain, the inverse power-law assumption for the grain-size distribution provides a functional, scaling relationship for the power-law dependence of attenuation on wavelength. The hypothesis that a single exponent can describe the grain-size distribution and the attenuation has not been proposed prior to this study, and the experimental evidence contained in this report serves to justify this theory.

The analysis of the log-log representations of the histograms indicates that an inverse power-law approximation is appropriate for nickel samples. The range of sizes measured (19.5 to 276 microns) gives the limits for the scaling relationship of the distribution.

The distinction between a self-similar distribution and an inverse power-law expression for the distribution is an important point to canvass. A power-law can be used for a self-similar distribution with an infinite range of sizes. It can also be used for a distribution with finite limits; i.e., a distribution which is not self-similar over all scales. The nickel samples used in this study, with a range of approximately 1.2 decades, fall into the second category for inverse power-law size distributions. This actuality is illustrated by no observations of self-similarity property after examination of different magnifications of the micrographs, as discussed in section VI.A. Another recommendation for future work is to investigate processing techniques or metals other than nickel that provide size distributions broad enough to allow examination of the grain structure at many magnifications, in order to reveal the self-similarity property of the size distribution.

The above discussion leads to another aspect of distributions. An inverse power-law is one appropriate function to use for distributions determined to be statistically self-similar. If the size distribution exists over many length scales but is not purely self-similar over all scales as in the case of multifractals [Feder 1988 p. 66], then other functions can be explored, including the log-normal. Section II reviewed the mathematical connections between the log-normal and inverse power-law functions. These two functions can be viewed as two members of a class of functions describing distributions which exist over a multitude of length scales. The ramifications of using other examples from this class of functions or combinations of power-laws with different exponents remains to be explored.

Rather than forcing a particular distribution function to fit a data set, a fundamental approach for choosing one distribution over another can be explored further. A deeper understanding of the underlying growth processes can be investigated as a means of anticipating the resulting grain-size distribution. Also, if the basic assumptions for selecting a particular distribution are known, then modifications are possible for different materials.

A current research topic in the area of growth processes is the study of cellular patterns and froth. Grain growth can be modeled in terms of the evolution of soap bubbles: as time progresses, some bubbles grow while others shrink, and the average number of sides and area per bubble are functions of time. This is an active topic of research [Flam 1989, Glazier & Stavans 1989, Weaire 1989], based on von Neumann's law and other equations relating pressure-driven diffusion in froths. These pursuits are directly applicable to the growth of grains in metals [Rhines & Patterson 1982, Doherty 1984]. Most of the existing analysis of froth is in terms of the time dependency of the number of sides and area per bubble, rather than the size distribution. Therefore, the connection between this type of endeavor and the results reported here are not straightforward at this point in time; nevertheless, it is a potential area for further development

While the experiments reported here were designed to test the agreement between the attenuation and grain-size distribution exponents, it was unanticipated that the attenuation exponents for the three samples would be nearly the same. It has been shown in a previous study that the attenuation exponent decreases as the percentage of recrystallization increases [Generazio 1988c]. It appears that for the samples used the extent of recrystallization is nearly the same for the three samples, resulting in approximately identical attenuation exponents. This observation allows

for examination of possible scaling relationships among the three annealing times for both attenuation and grain-size distribution, as shown in section VI.D. One promising direction is to explore the nondestructive evaluation of grain-size distribution using this property for a series of metal samples with the same exponent. If the size distribution is known for *one* sample (either a priori or through a destructive measurement), then the size distributions for all of the other samples could be determined by measuring the relative shifts of the attenuation.

One possible justification for assuming that the exponents does not vary for the three samples comes from small angle scattering analysis. It has been hypothesized that the exponent derived from the small angle scattering curves is a signature of the growth mechanism for silica particle aggregation, and is dependent upon the growth process [Kjems et. al. 1986]. While this consideration is beyond the scope of this report, a potential future research direction is to investigate the possibility that the grain-size distribution exponent is constant for specific types of grain growth.

One of the drawbacks to the analysis of the effect of the grain-size distribution on mechanical properties has been the measurement of grain size. As mentioned in section II, "The near absence of recognition of these features and of their effects on properties is understandable in view of the great amount of labor required in the experimental measurement of grain volume distribution..." [Rhines & Patterson 1982]. It is therefore suggested that ultrasonic attenuation measurement may prove to be an appropriate grain-size distribution measurement for materials, as it is shown to be for pure nickel, and can be used to gain a deeper understanding of the grain-size distribution by physical metallurgists.

The theoretical and experimental work presented here are directed toward nondestructive measurement of the exponent of an inverse power-law expression for the grain-size distribution. It can be suggested that the corners or crossovers of the attenuation, as discussed in section V.B, are approximate measurements of the upper and lower size limits. To accomplish this, a broad span of wavelengths is required, with a span much wider than the grain-size distribution in order to determine the corners. While this is experimentally feasible, the problem of finding the exact values for the limits remains. In any event, if the limits are known, then any statistical moment can be calculated, including the average grain size:

$$\bar{D} = K\frac{D_2^{2-\gamma} - D_1^{2-\gamma}}{2 - \gamma} \tag{53}$$

Thus the nondestructive measurement of the largest and smallest grain size using very broadband attenuation measurements is a future application of this theory.

A major thrust of nondestructive testing has been flaw detection in metals using ultrasonic analysis. The ongoing research implicitly requires knowledge of grain boundary scattering in order to detect and accurately locate a flaw site. This application of ultrasonic analysis treats grain boundary scattering as the noise source, and models for the scattering are used to improve detection schemes. For example, the magnitude spectrum for grain boundary echoes has been expressed as [Shankar et. al. 1986]

$$\text{Magnitude spectrum} \sim f^2 e^{-bf} \tag{54}$$

where b is a constant. The derivation of this expression assumes that the attenuation due to scattering is dependent upon the fourth power of frequency and that the absorption effects are significant. The theoretical work continues by finding an expression for the magnitude spectrum from the flaw signal, and then band-pass filters and accompanying algorithms are used to suppress the grain noise. More appropriate expressions for the grain boundary scattering may improve the development and analysis of the signal processing techniques used for flaw detection.

In conclusion, the progress outlined in this report makes several contributions to the understanding of attenuation in metals from a number of perspectives. The work presented here

establishes that the scaling properties of grain size and ultrasonic attenuation are related, and the attenuation exponent is shown to be an appropriate nondestructive measurement of the grain-size distribution exponent, as validated by the experimental evidence using pure nickel. A further scaling relationship for the annealing duration is shown to exist, implying the possibility of more extensive nondestructive evaluation for samples with identical exponents. These analysis techniques have implications for both grain size determination and flaw detection in metals. Future endeavors may include examination of other candidate materials for the scaling relationships offered here; such an undertaking is indicated and justified by the positive results obtained in this study.

Bibliography

Atkinson, H. V. ,"Theories of Normal Grain Growth in Pure Single Phase Systems," Acta. Met., 36, pp. 469-491, 1988.

Bhatia, A. B., "Scattering of High-Frequency Sound Waves in Polycrystalline Materials," Journal of the Acoustical Society of America, 31, pp. 16-23, January, 1959a.

_____, R. A. Moore, "Scattering of High Frequency Sound Waves in Polycrystalline Materials. II," Journal of the Acoustical Society of America, 31, pp. 1140-1142, 1959b.

Bozorg-Grayeli, N., Acoustic Nondestructive Evaluation of Microstructure, Ph.D. Thesis, Stanford University, 1981.

DeHoff, R. T., "The Estimation of Particle-Size Distributions from Simple Counting Measurements Made on Random Plane Sections," Transactions of the Metallugical Society of AIME, 233, pp. 25-29, 1965.

_____, Quantitative Microscopy, New York: McGraw-Hill, 1968.

Dieter, G. E. Jr., Mechanical Metallurgy, New York: McGraw-Hill, 1961.

Doherty, R. D., "Stability of the Grain Structure in Metals," Journal of Materials Education, 6, pp. 845-883, 1984.

Feder, J., Fractals, New York: Plenum Press, 1988.

Feltham, P., "Grain Growth in Metals," Acta Metallurgica, 5, pp. 97-105, 1957.

Flam, F., "Frothy Physics," Science News, 136, 72-76, July 29, 1989.

Generazio, E. R., "The Role of the Reflection Coefficient in Precision Measurement of Ultrasonic Attenuation," Materials Evaluation, 43, pp. 995-1004, 1985.

_____, "Scaling Attenuation Data Characterizes Changes in Material Microstructure," Materials Evaluation, 44, pp. 198-208, 1986.

_____, "Determination of Grain-Size Distribution Function Using Two-Dimensional Fourier Transforms of Tone-Pulse-Encoded Images," Materials Evaluation, 46, pp. 528-534, 1988b.

_____, "Ultrasonic Attenuation Measurements Determine Onset, Degree, and Completion of Recrystallization," Materials Evaluation, 46, pp. 1198-1203, 1988c.

Glazier, J. A., J. Stavans, "Nonideal Effects in the Two-Dimensional Soap Froth," Physical Review A, 40, pp. 7398-7401, 1989.

Kaye, B. H., A Random Walk Through Fractal Dimensions, New York: VCH Publishers, 1989.

Kjems, J. K., T. Freltoft, D. Richter, S. K. Sinha, "Neutron Scattering from Fractals," Physics, 136B, pp. 285-290, 1986.

Klinman, R., E. T. Stephenson, "Ultrasonic Prediction of Grain Size and Mechanical Properties in Plain Carbon Steel," Materials Evaluation, 39, pp. 1116-1120, 1981.

Krautkraemer, J., H. Krautkraemer, Ultrasonic Testing of Materials, 2d ed., New York: Springer-Verlag, 1983.

Kumar, S., A. K. Govil, "Ultrasonic Attenuation in AC/HT-2 Steel," Indian Journal of Technology, 18, pp. 197-202, 1980.

Lifshitz, E. M., G. D. Parkhomovskii, Zh. Eksp Teor. Fiz., 20, pp. 175-182, 1950.

Mandelbrot, B. B., The Fractal Geometry of Nature, New York: W. H. Freeman and Company, 1983.

Martin, J. E., "Scattering Exponents for Polydisperse Surface and Mass Fractals," Journal of Applied Crystallography, 9, pp. 25-27, 1986.

_____, J. P. Wilcoxon, "Critical Dynamics of the Sol-Gel Transition," Physical Review Letters, 61, pp. 373-376, 1988.

Mason, W. P., H. J. McSkimin, "Attenuation and Scattering of High Frequency Sound Waves in Metals and Glasses," Journal of the Acoustical Society of America, 19, pp. 464-473, 1947.

_____, H. J. McSkimin, "Energy Losses of Sound Waves in Metals Due to Scattering and Diffusion," Journal of Applied Physics, 19, pp. 940-946, 1948.

Mercier, N., "Ultrasonic Classification of Metals by Grain Size," Ultrasonics International 1975 Conference Proceedings, pp. 64-67, 1975.

Merkulov, L. G., Sov. Phys. Tech. Phys. (English transl.), 1, pp. 59-69, 1956.

Montroll, E. W., M. F. Shlesinger, "Maximum Entropy Formalism, Fractals, Scaling Phenomena, and 1/f Noise: A Tale of Tails," Journal of Statistical Physics, 32, pp. 209-230, 1983.

Nicoletti, D., Scaling Properties of Ultrasonic Attenuation and Grain Size in Metals, Ph.D. Thesis, Drexel University, 1991.

Oppenheim, A. V., A. S. Willsky, Signals and Systems, Englewood Cliffs, New Jersey: Prentice-Hall, 1983.

Orbach, R., "Dynamics of Fractal Networks," Science, 231, pp. 814-819, 1986.

Papadakis, E. P., "Grain-Size Distribution in Metals and its Influence on Ultrasonic Attenuation Measurements," Journal of the Acoustical Society of America, 33, pp. 1616-1621, 1961.

_____, E. L. Reed, "Ultrasonic Detection of Changes in the Elastic Properties of a 70-30 Iron-Nickel Alloy upon Heat Treatment," Journal of Applied Physics, 12, pp. 682-687, 1961.

_____, "Ultrasonic Attenuation and Velocity in Three Transformation Products in Steel," Journal of Applied Physics, 35, pp. 1474-82, 1963.

_____, "From Micrograph to Grain-Size Distribution with Ultrasonic Applications," Journal of Applied Physics, 35, pp. 1586-1594, 1964.

_____, "Revised Grain-Scattering Formulas and Tables," Journal of the Acoustical Society of America, 37, pp. 703-710, 1965a.

_____, "Ultrasonic Attenuation Caused by Scattering in Polycrystalline Metals," Journal of the Acoustical Society of America, 37, pp. 711-717, 1965b.

_____, "Ultrasonic Attenuation and Velocity in SAE 52100 Steel Quenched from Various Temperature," Metallurgical Transactions, pp. 1053-1057, 1970.

Rayleigh, Lord, Theory of Sound, London: Macmillan, 1894.

Rhines, F. N., B. R. Patterson, "Effect of the Degree of Prior Cold Work on the Grain Volume Distribution and the Rate of Grain Growth of Recrystallized Aluminum," Metallurgical Transactions A, 13A, pp. 985-993, 1982.

Roderick, R. L., R. Truell, "The Measurement of Ultrasonic Attenuation in Solids by the Pulse Technique and Some Results in Steel," Journal of Applied Physics, 23, pp. 267-279, 1952.

Roney, R. K., The Influence of Metal Grain Size on the Attenuation of an Ultrasonic Wave, Ph.D. thesis, California Institute of Technology, 1950.

Roth, W., "Scattering of Ultrasonic Radiation in Polycrystalline Metals," Journal of Applied Physics, 19, pp. 901-910, 1948.

Sander, L. M., "Fractal Growth," Scientific American, 256, pp. 94-102, 1987.

Saniie, J., N. M. Bilgutay, "Quantitative Grain Size Evaluation Using Ultrasonic Backscattered Echoes," Journal of the Acoustical Society of America, 80, pp. 1816-1824, 1986.

_____, T. Wang, N. M. Bilgutay, "Statistical Evaluation of Backscattered Ultrasonic Grain Signals," Journal of the Acoustical Society of America, 84, pp. 400-408, 1988.

Seemann, H. J., W. Bentz, "Untersuchungen uber den Einflufs des Geguges auf die Extinktion von Ultraschallwellen in metallischen Stoffen," Z. Metallkde., 45, pp. 663-669, 1954.

Serabian, S., R. S. Williams, "Experimental Determination of Ultrasonic Attenuation Characteristics Using the Roney Generalized Theory," Materials Evaluation, 36, pp. 55-62, 1978.

Shankar, P. M., U. Bencharit, N. M. Bilgutay, J. Saniie, "Grain Noise Suppression through Bandpass Filtering," Materials Evaluation, 46, pp. 1100-1104, 1988.

Smith, R. L., W. N. Reynolds, H. N. G. Wadley, "Ultrasonic Attenuation and Microstructure in Low-Carbon Steels," Metal Science, 15, pp. 554-558, 1981.

_____, "The Effect of Grain Size Distribution on the Frequency Dependence of the Ultrasonic Attenuation in Polycrystalline Materials," Ultrasonics, 20, pp. 211-214, 1982.

_____, "Ultrasonic Materials Characterization," NDT International, 20, pp. 43-48, 1987.

Wegel, R. L., H. Walther, "Internal Dissipation in Solids for Small Cyclic Strains," Physics, 6, pp. 141-157, 1935.

Weaire, D., "A Note on the Elastic Behaviour of Ordered Hexagonal Froth," Philosophical Magazine Letters, 60, pp. 27-30, 1989.

West, B. J., A. L. Goldberger, "Physiology in Fractal Dimensions," American Scientist, 75, pp. 354-365, 1987.

_____, M. F. Shlesinger, "On the Ubiquity of 1/f Noise," International Journal of Modern Physics B, 3, pp. 795-819, 1989.

Figures

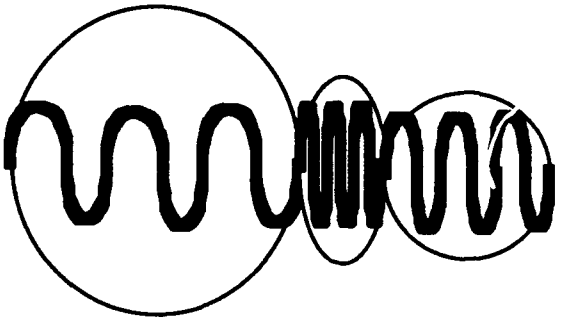

Figure 1: Tone-pulse encoding for three grains

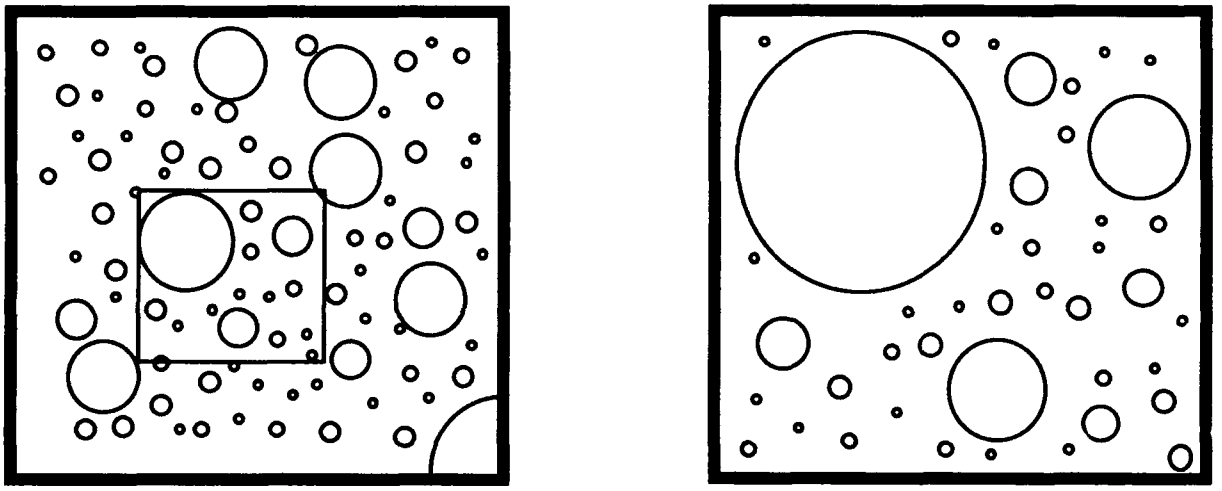

Figure 2: Circles of various sizes, shown at two magnifications

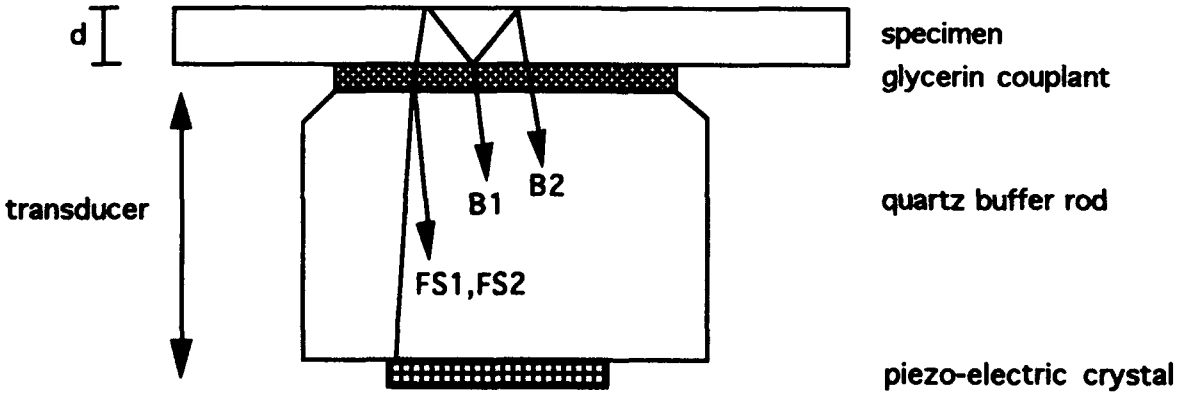

Figure 3: Experimental Set-up for Attenuation Measurement

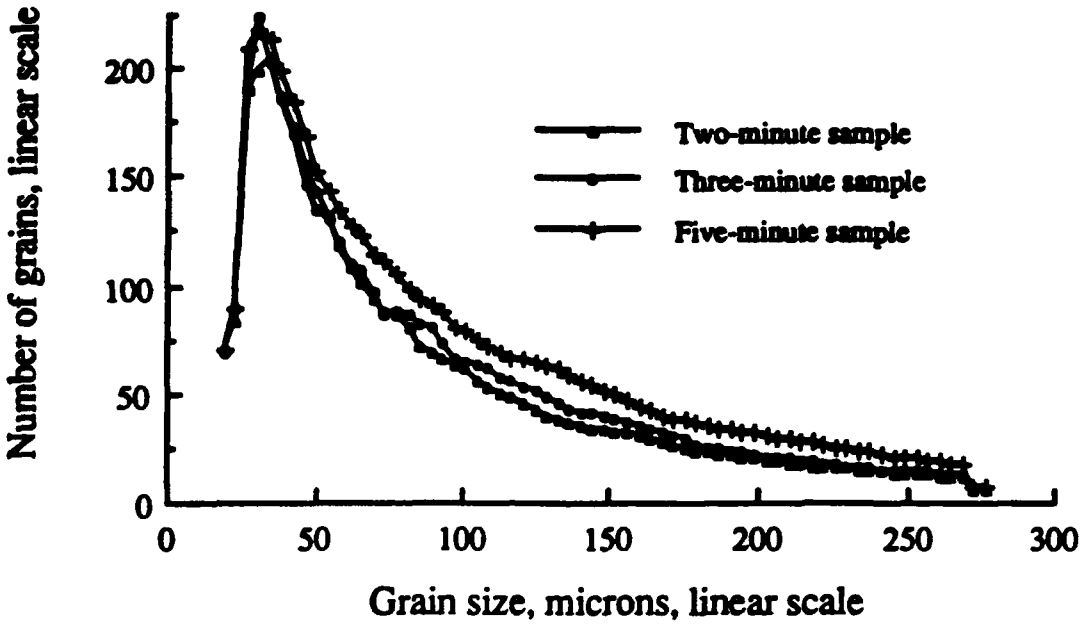

Figure 4a Grain size histograms for the two-, three- and five-minute samples
Linear-linear scale

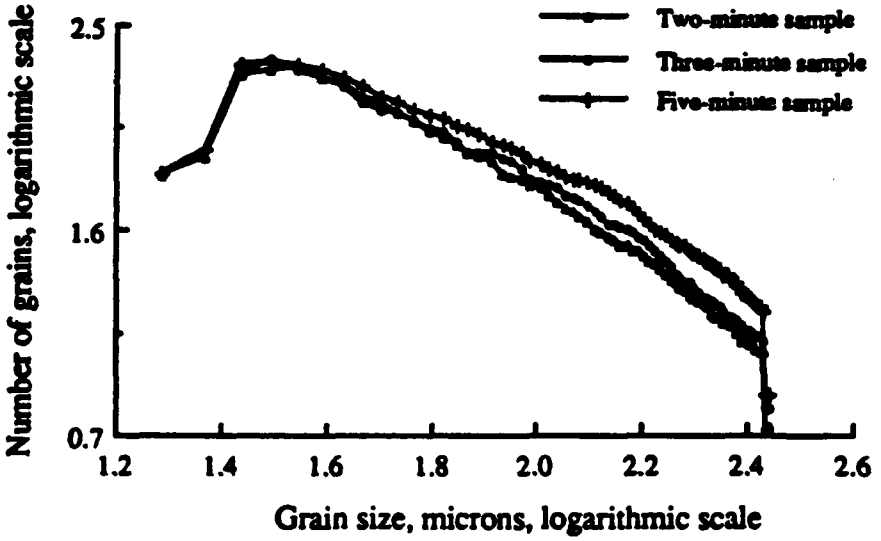

Figure 4b Grain size histograms for the two-, three- and five-minute samples
Log-log scale

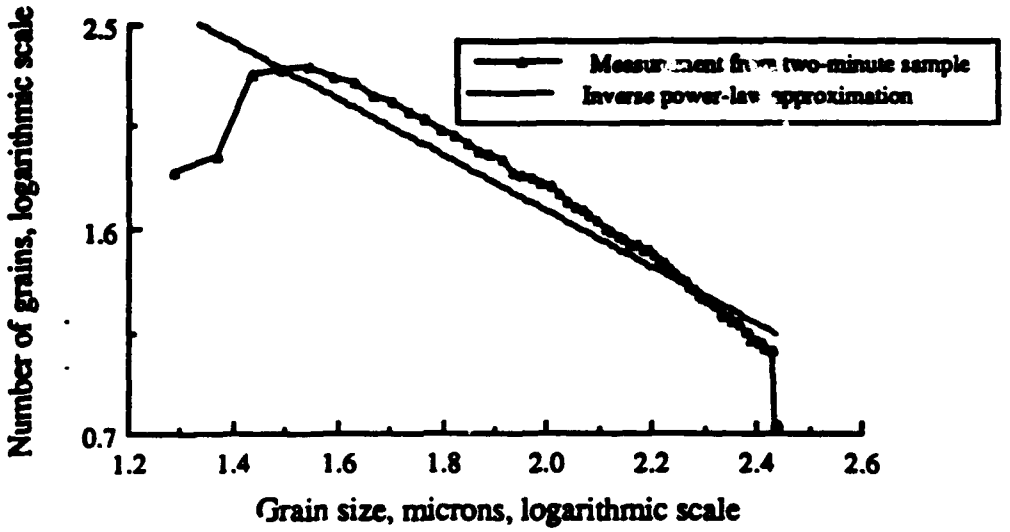

Figure 5a Inverse power-law approximation based on entire data set and measured values for the grain size histogram for the two-minute sample
Log-log scale

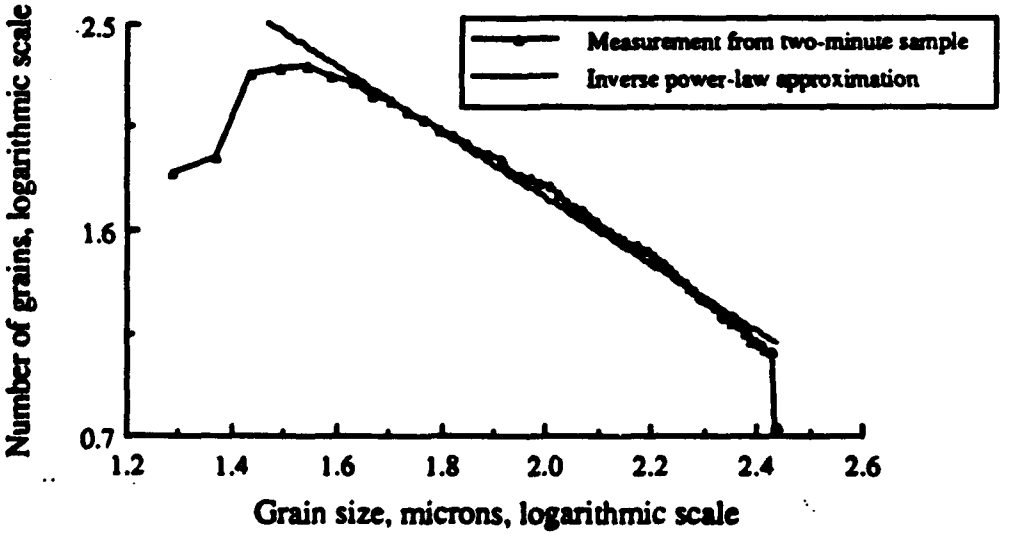

Figure 5b Inverse power-law approximation based on partial data set and measured values for the grain size histogram for the two-minute sample
Log-log scale

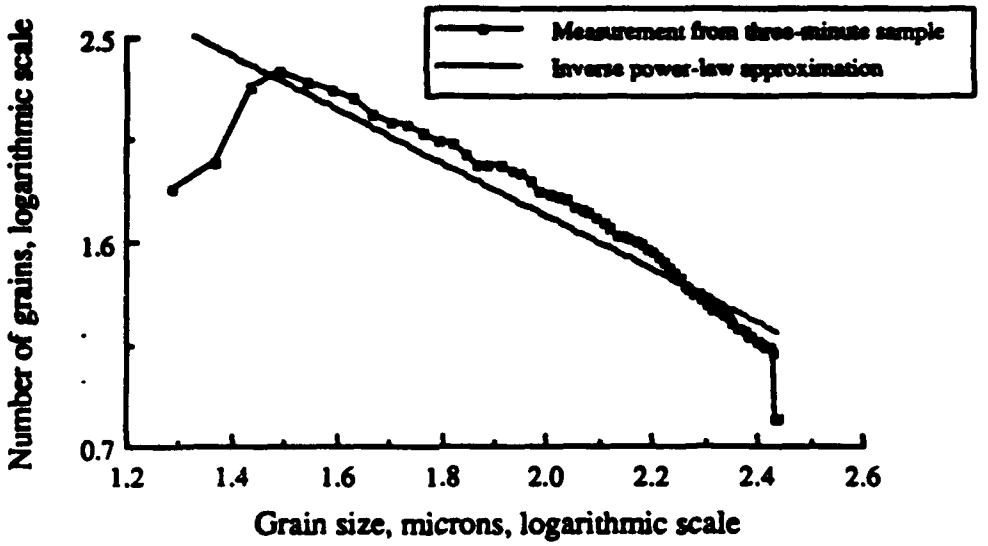

Figure 6a Inverse power-law approximation based on entire data set and measured values for the grain size histogram for the three-minute sample
Log-log scale

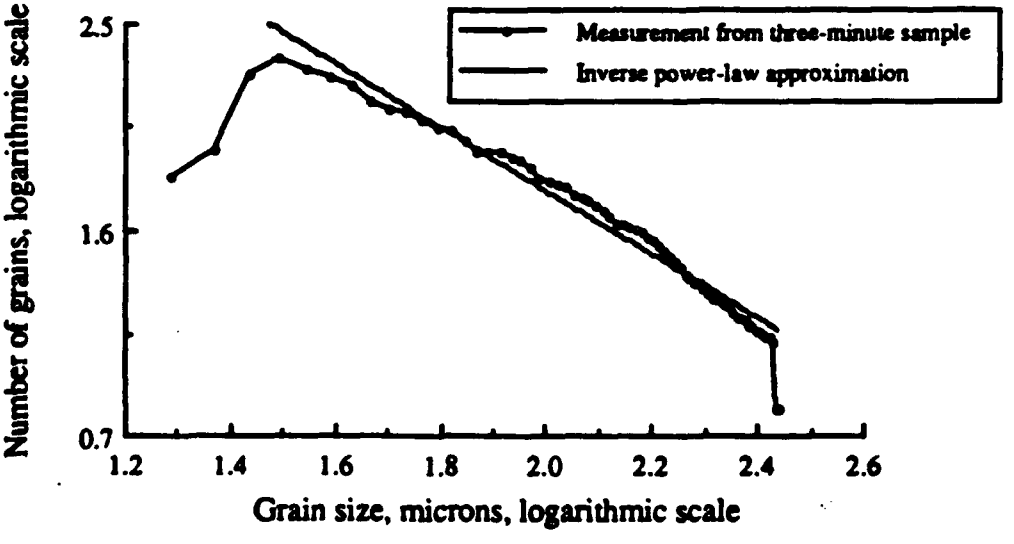

Figure 6b Inverse power-law approximation based on partial data set and measured values for the grain size histogram for the three-minute sample
Log-log scale

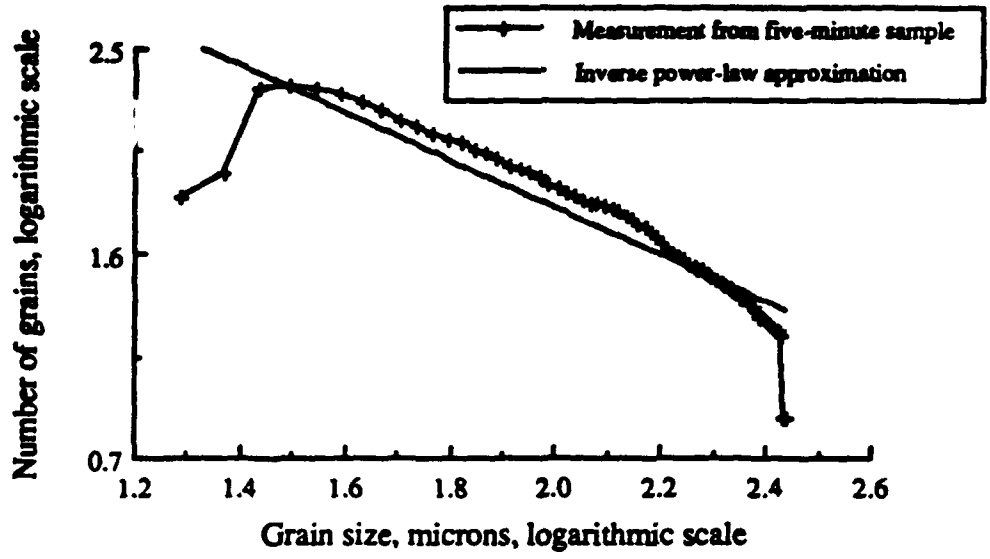

Figure 7a Inverse power-law approximation based on entire data set and measured values for the grain size histogram for the five-minute sample
Log-log scale

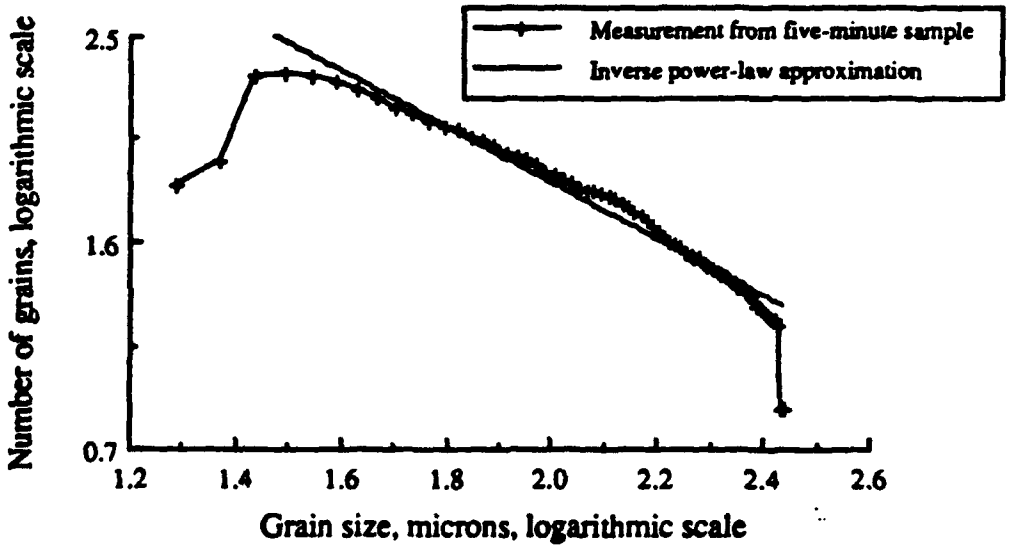

Figure 7b Inverse power-law approximation based on partial data set and measured values for the grain size histogram for the five-minute sample
Log-log scale

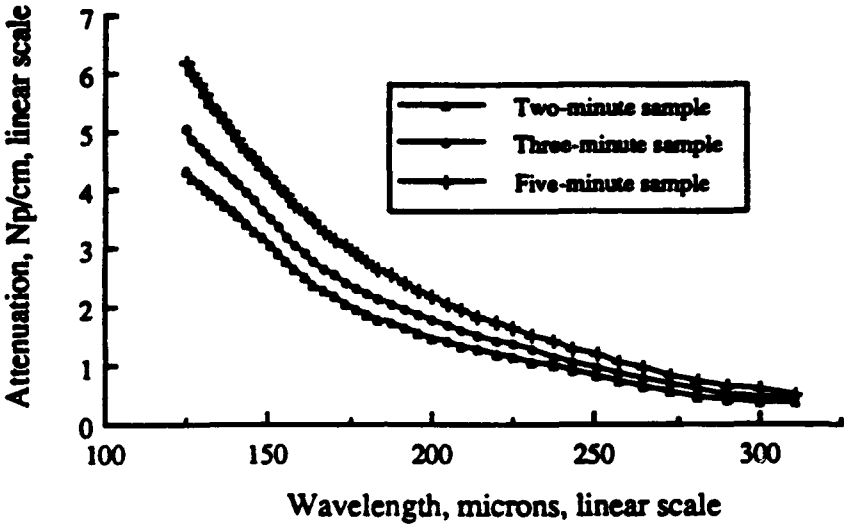

Figure 8a Averaged attenuation measurement for the two-, three- and five-minute samples
Linear-linear scale

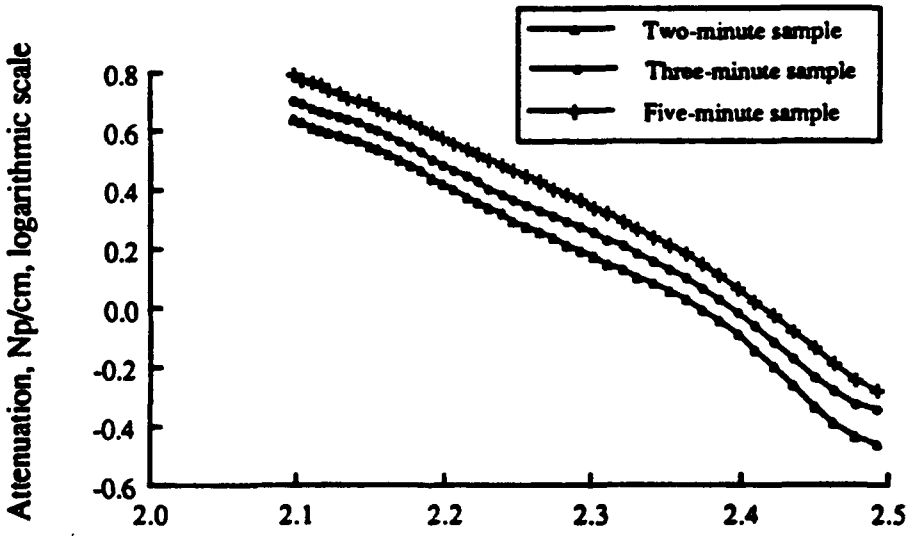

Figure 8b Averaged attenuation measurement for the two-, three- and five-minute samples
Log-log scale

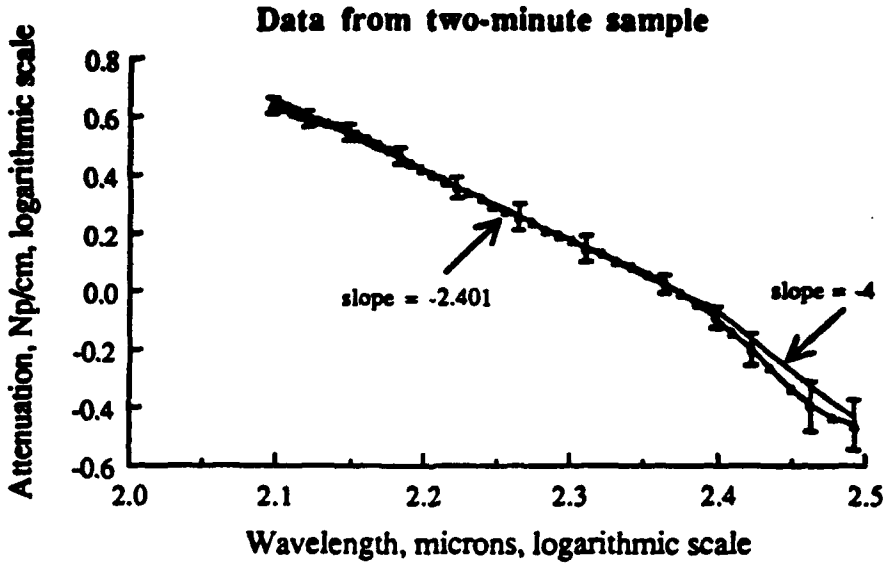

Figure 9 Linear approximation and measured values for the attenuation with error bars for the two-minute sample
Log-log scale

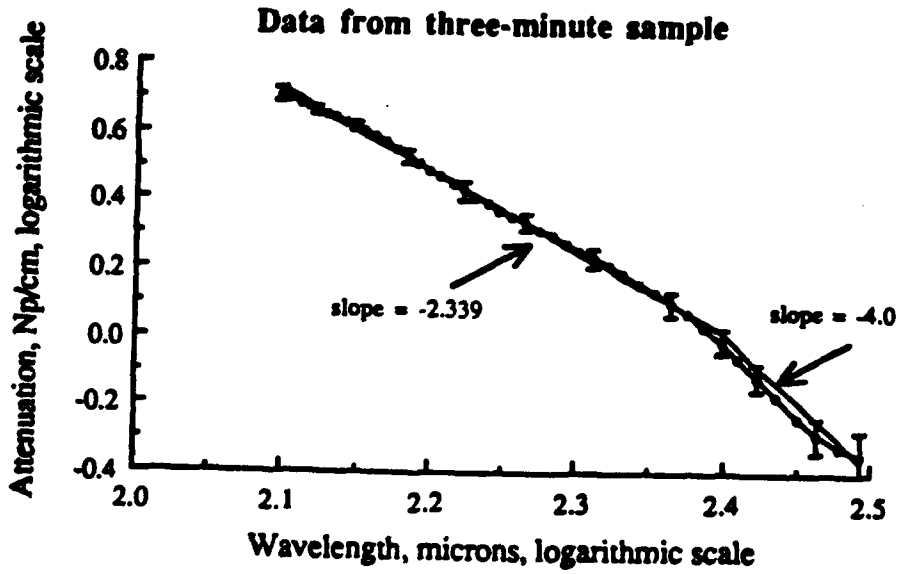

Figure 10 Linear approximation and measured values for the attenuation with error bars for the three-minute sample
Log-log scale

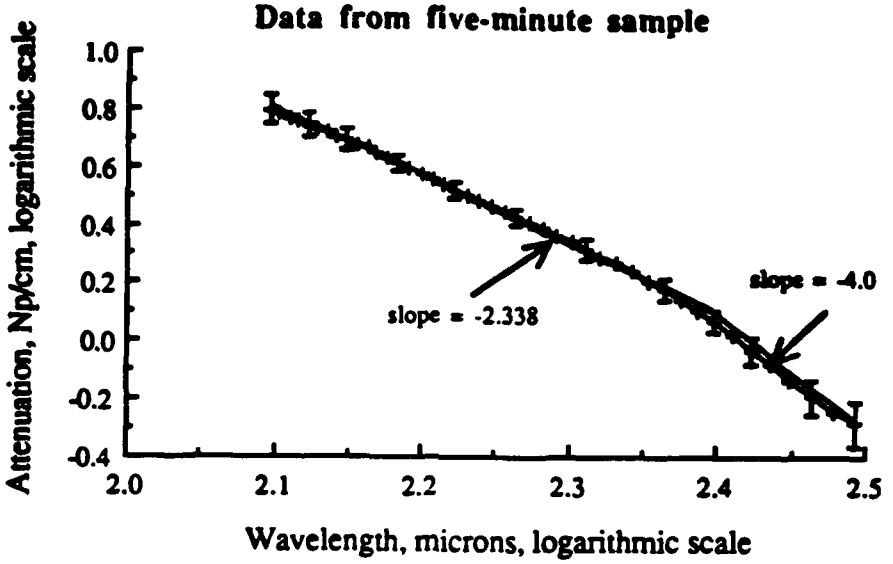

Figure 11 Linear approximation and measured values for the attenuation with error bars for the five-minute sample
Log-log scale

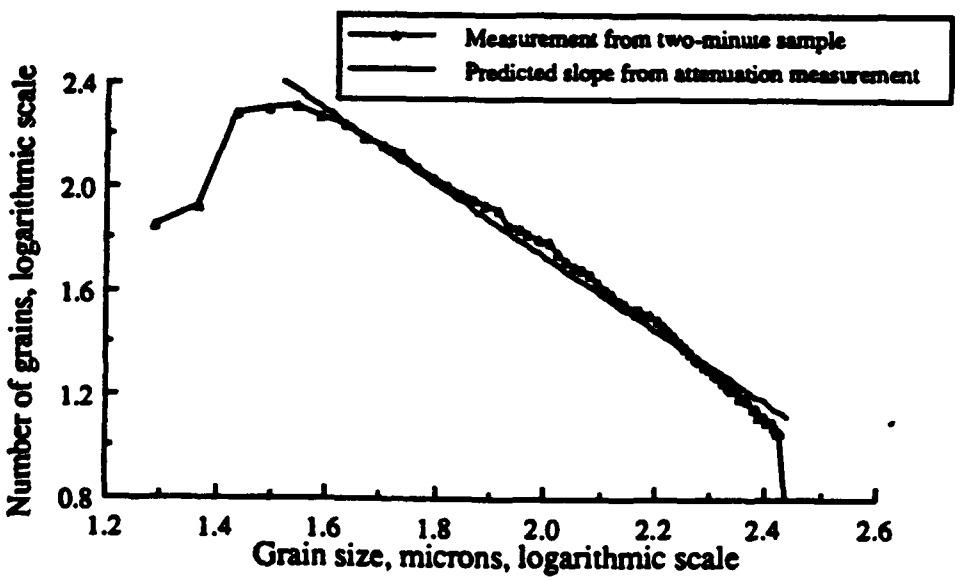

Figure 12 Slope predicted by attenuation results and measured values for the grain size histogram for the two-minute sample
Log-log scale

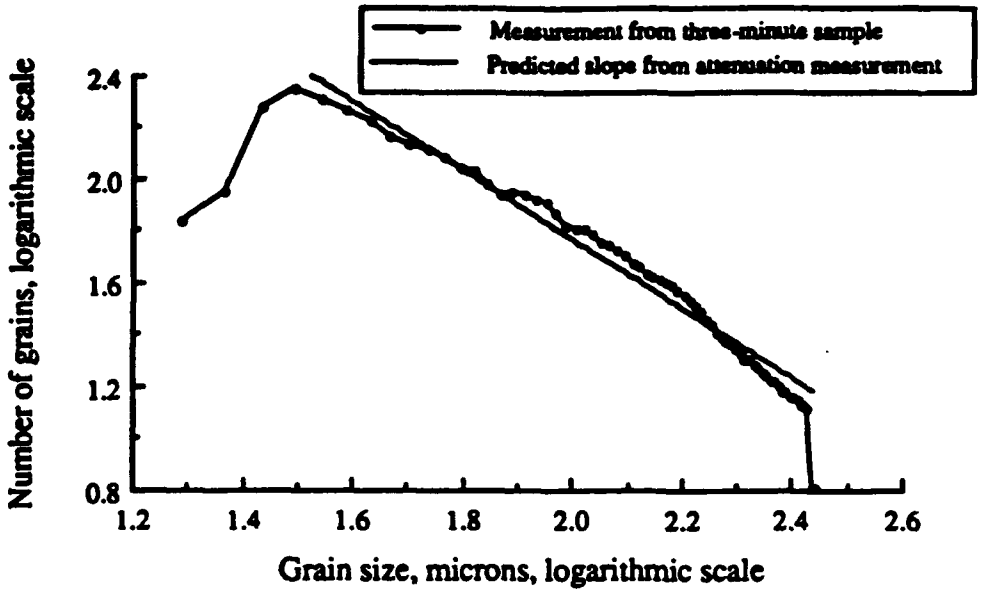

Figure 13 Slope predicted by attenuation results and measured values for the grain size histogram for the three-minute sample
Log-log scale

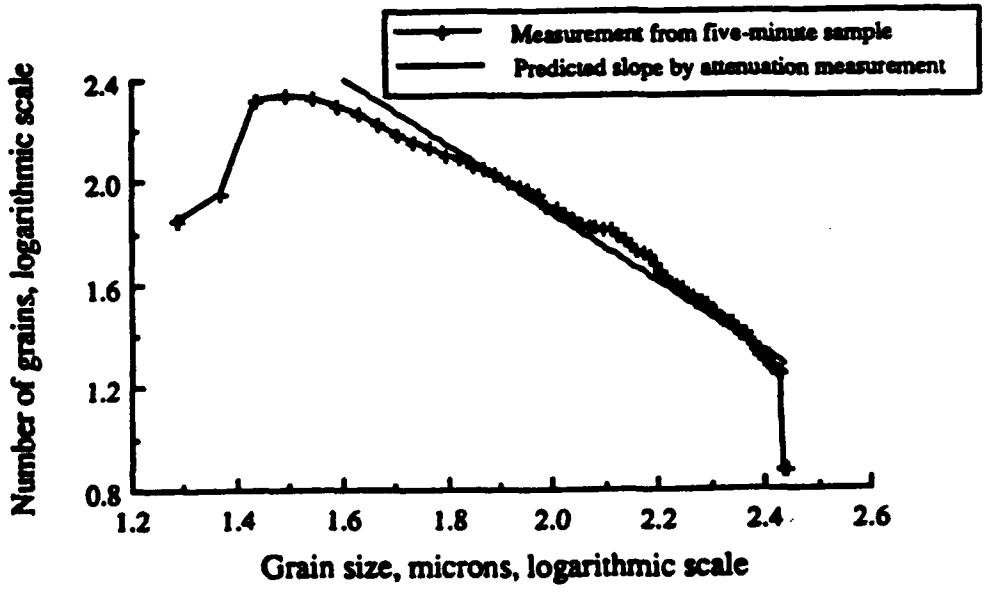

Figure 14 Slope predicted by attenuation results and measured values for the grain size histogram for the five-minute sample
Log-log scale

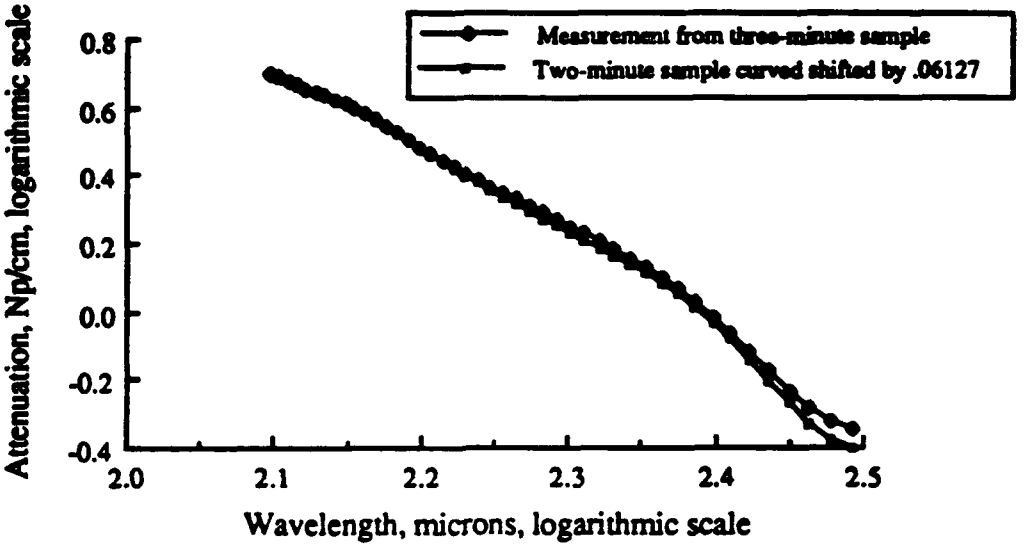

Figure 15 Measured attenuation for two-minute sample shifted by 0.06127 and measured values for the attenuation for the three-minute sample
Log-log scale

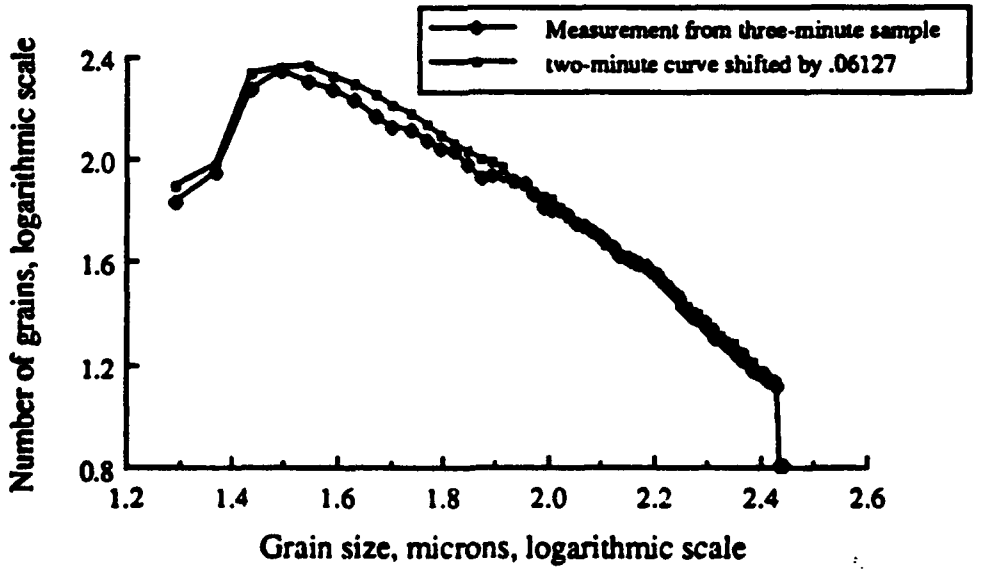

Figure 16 Measured attenuation for two-minute sample shifted by 0.14665 and measured values for the attenuation for the five-minute sample
Log-log scale

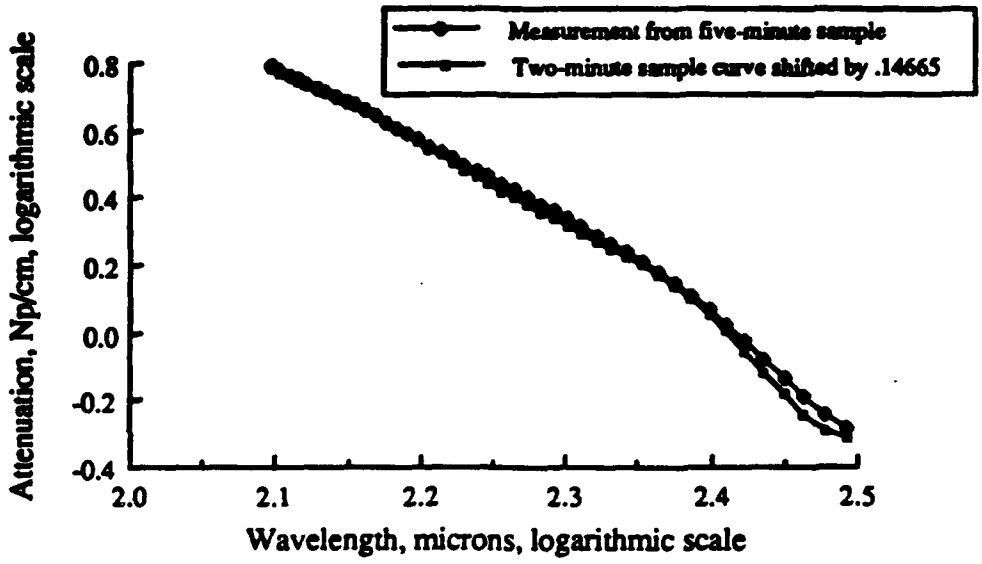

Figure 17 Measured grain size histogram for two-minute sample shifted by 0.06127 and measured values for the grain size histogram for three-minute sample Log-log scale

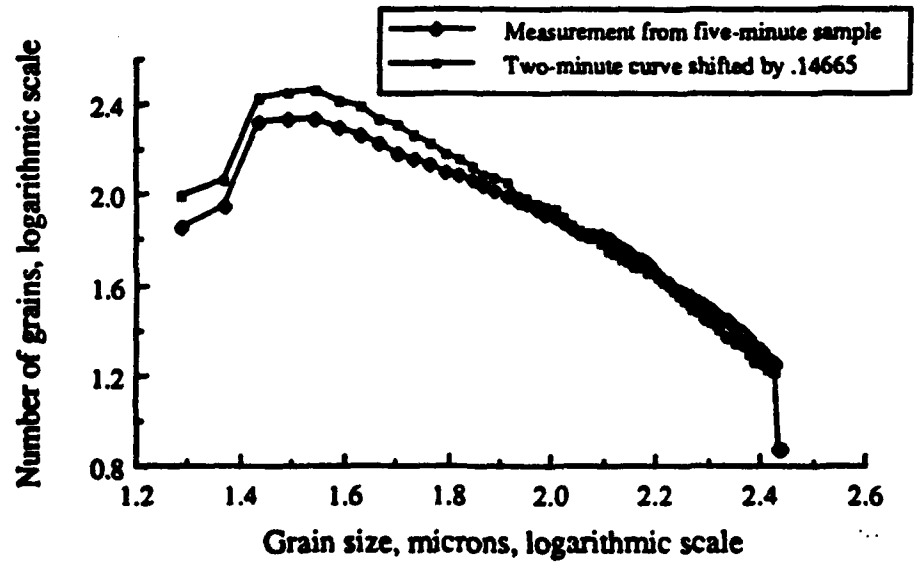

Figure 18 Measured grain size histogram for two-minute sample shifted by 0.14665 and measured values for the grain size histogram for five-minute sample Log-log scale